International Journal Of
Industrial Electronics Control and Optimization
Print ISSN: 3517-2645
Online ISSN: 3568-2645
Homepage: https://ieco.usb.ac.ir/

Adaptive Backstepping Control of two-group SEIAR Epidemic Model in the Presence of Input Saturation and External Disturbances

Fariba Nobakht[1] | Hussein Eliasi[2]

Faculty of Electrical and Computer Engineering, University of Birjand, Birjand, Iran.[1,2]
Corresponding author's email: h_eliasi@birjand.ac.ir

Article Info

Article type:
Research Article

Article history:
Received: 2024-11-03
Received in revised form: 2025-02-01
Accepted: 2025-02-19
Published online: 22-Dec-2025

Keywords:
Backstepping sliding mode control,
Input saturation,
Nonlinear adaptive control,
SEIAR mathematical model.

ABSTRACT

This paper proposes a robust adaptive control strategy based on integral backstepping for nonlinear epidemic systems under input saturation, model uncertainties, and external disturbances. The proposed method combines backstepping for systematic control design, sliding mode control for robustness, and adaptive control to handle unknown parameters dynamically. To address input saturation, a novel auxiliary design system combined with Nussbaum gain functions is introduced, mitigating saturation effects and ensuring stability. The epidemic dynamics are modeled using the SEIAR framework, which includes Susceptible, Exposed, Infected, Asymptomatic, and Recovered populations. The controller employs three control inputs—vaccination, social distancing measures, and treatment of infected individuals—to drive the populations of susceptible, exposed, and infected individuals to zero. Simulation results demonstrate that the proposed control scheme effectively eliminates infections, ensuring that the recovered population converges to the total population size. The method provides precise trajectory tracking despite input constraints and external disturbances. These findings highlight its strong potential for real-world epidemic management, particularly in resource-limited and uncertain environments.

I. Introduction

Mathematical modelling plays a vital role in enhancing our understanding of how infectious diseases spread. By breaking down the complex mechanisms of disease transmission, epidemic models offer valuable insights into the dynamics and patterns of outbreaks [1]. These models not only forecast the progression of epidemics—such as the number of infections, hospitalizations, and fatalities—but also assess the effectiveness of various control measures [2].

Traditional epidemic models (see e.g., [3], [4]) often assume that all individuals share the same susceptibility to infection and follow uniform transmission dynamics. However, factors such as age, gender, community, education level, and geographic location can significantly impact disease spread. To better capture these dynamics, populations are categorized into distinct groups, each with specific epidemic parameters. This approach, represented by multi-group epidemic models, has been extensively studied and provides a more accurate understanding of disease spread within and between groups (see e.g., [5], [6], [7]) . These models offer valuable insights for designing more effective strategies to control and prevent infectious diseases.

Various strategies have been implemented to control epidemics, including social distancing, lockdowns, hygiene practices, face masks, laboratory testing, contact tracing, and monitoring infected or exposed individuals. To optimize these measures, researchers have developed different controllers for infectious disease models. Optimal control theory has been used to evaluate interventions aimed at reducing disease transmission, considering both ongoing and final costs over finite or infinite time horizons (see e.g., [5], [8], [9], [10], and [11]).

Optimal control strategies typically assume full knowledge of all dynamic terms and parameters. However, pandemic model parameters—such as disease spread, mortality, and contact rates—are inherently uncertain and influenced by social and disease-related factors [12]. These

Copyright © H. Eliasi(s).
Publisher: University of Sistan and Baluchestan

unknown variables must be accounted for when designing outbreak control measures. To tackle this, robust and adaptive control techniques are used to maintain stable performance despite uncertainties within the model [13, 14, 15].

Sliding mode control (SMC) is a robust technique for managing nonlinear systems, offering resilience against parameter variations and disturbances [14]. However, the conventional SMC approach, which uses the sign function for switching, can cause chattering—an undesirable phenomenon that can destabilize the system. To mitigate this, several techniques have been developed, including boundary layer methods, hysteresis-based approaches, alternative switching functions like saturation, and higher-order sliding mode control [16].

Backstepping is a structured method for designing tracking and regulation strategies, particularly for "strict-feedback" systems. It employs a recursive process where state variables are treated as virtual controls. However, this approach lacks robustness against parametric variations. By integrating sliding mode control, backstepping effectively addresses parameter uncertainties and enhances system stability [17, 18, 19]. This combined method divides the nonlinear system into subsystems, applying sliding mode control to each while using the Lyapunov function to ensure the convergence of position-tracking errors under any initial condition.

The integrator backstepping technique offers significant advantages by transforming nonlinear systems into a strict-feedback form [19, 16]. When paired with sliding mode control, it minimizes chattering in the control input and improves robustness against modeling uncertainties and external disturbances. Furthermore, incorporating an integrator within the control structure enhances precision in achieving steady-state control, making this approach highly effective for a wide range of applications.

Input saturation is a prevalent challenge in real-world control systems, where control inputs are constrained by physical or practical limitations. In the context of epidemic disease management, input saturation occurs when health systems are overwhelmed and unable to respond effectively or promptly to outbreaks. This can result from various factors, including sudden surges in cases, lack of preparedness, limited availability of resources, and social or behavioral resistance to interventions. For example, inadequate infrastructure, insufficient training, and poor coordination among healthcare providers can lead to critical shortages of medical supplies, personnel, and facilities. Additionally, public reluctance to adopt measures such as vaccination or social distancing can further undermine the effectiveness of control strategies. These limitations introduce significant nonlinearities into epidemiological models, making it difficult to accurately predict the spread and impact of diseases. Addressing actuator saturation is therefore essential for developing reliable models that can inform effective decision-making.

To tackle input constraints, anti-windup compensator (AWC) techniques are employed to maintain system stability and performance under saturation conditions. By incorporating anti-windup mechanisms, controllers can adapt to input limitations, ensuring accurate regulation of system behavior and reliable predictions despite actuator constraints. Anti-windup controller techniques are broadly categorized into two approaches: one-step and two-step design procedures. One-step approaches develop feedback controllers that inherently account for input saturation, while two-step procedures involve designing an optimal controller without considering saturation initially and later augmenting it with anti-windup compensation [20, 21]. These methods enhance the robustness of control systems, enabling effective management of epidemics even under resource limitations

Various strategies have been proposed to design anti-windup controllers for addressing input saturation challenges. These include adaptive backstepping control algorithms [22], sliding mode tracking control methods [23], and terminal sliding mode controllers for systems with unknown uncertainties and input saturation constraints [24]. Additionally, integral backstepping sliding mode control approaches have been developed for systems like unmanned autonomous helicopters [16]. These methods aim to ensure that systems with saturating actuators closely replicate the performance of their unsaturated counterparts, enhancing reliability and stability.

This article introduces a novel nonlinear anti-windup control method that combines backstepping with adaptive sliding mode control (ABSMC) to stabilize a nonlinear multi-input, multi-output (MIMO) system under input saturation, modelling uncertainties, and external disturbances. The anti-windup compensator is designed using a one-step strategy to address challenges arising from input limitations in real-world scenarios. To manage input saturation and prevent actuator failures, an auxiliary system is incorporated.

Input saturation, being a non-smooth function, poses a challenge for backstepping, which requires differentiable functions. To address this, a continuous approximation is used to estimate the saturation, ensuring a controlled approximation error and enabling the system to be expanded for controller development. However, managing the derivative of the estimated function introduces additional complexity, which is resolved using a Nussbaum function. The Nussbaum function serves as a powerful mathematical tool, effectively addressing the nonlinearities introduced by input saturation. It ensures the stability and positivity of system states while also enhancing the robustness of the controller. By working in conjunction with the auxiliary design system, the Nussbaum function contributes to a

resilient and adaptive control scheme capable of maintaining stability and performance even under challenging conditions. The controller is applied to a bi-model epidemic, which includes five groups of individuals and three control methods: vaccination, antiviral treatment, and social distancing. The controller seeks to reduce the number of susceptible, infected, and exposed individuals to zero, even under input saturation, which also minimizes the number of asymptomatic individuals. Meanwhile, the recovered population stabilizes at its peak level, aligning with the overall population trend. Compared to existing research on the control of epidemiological systems, this work makes several significant contributions:

a. A robust adaptive backstepping sliding mode controller has been developed to manage MIMO epidemic systems affected by input saturation, time-varying external disturbances, and uncertainties.

b. Multigroup epidemic models provide more detailed and accurate information about disease spread compared to models that treat the population as a whole. This richer information can guide better decisions regarding the control and prevention of infectious diseases.

c. The controller accounts for uncertainties in the nonlinear dynamics of the epidemic model, allowing it to adapt to variations and unexpected changes in the disease transmission process. This enhances control performance and resilience in real-world scenarios.

d. The proposed control approach introduces a novel auxiliary design system and Nussbaum gain functions to address actuator saturation. These techniques ensure effective management of input saturation, enabling the controller to achieve the desired objectives despite input constraints.

e. The model incorporates a time-varying total population ($\dot{N}(t) \neq 0$) and includes critical factors such as birth and natural death rates, as well as the loss of immunity in recovered individuals over time. These factors significantly influence disease dynamics and the effectiveness of control measures.

The remainder of this paper is organized into five sections. Section II introduces and provides a detailed explanation of the dynamic two-group SEIAR model, including a proof of the results related to its positivity property. This property is crucial to the system, as it ensures that negative populations do not occur at any time. Section III focuses on the design of the adaptive backstepping sliding mode control for the MIMO nonlinear system. In Section IV, we present numerical simulation results that demonstrate the applicability of the proposed anti-windup control approach to the nonlinear model. Finally, Section V concludes the paper.

II. Nonlinear Two-group SEIAR Model

Multi-group epidemic models are mathematical frameworks that divide a population into multiple groups based on specific characteristics, such as age, gender, education level, occupation, and risk factors, among others. Each group is assumed to have its own set of parameters related to disease transmission, susceptibility, and recovery. The proposed SEIAR epidemic model builds upon the traditional SEIR model, as outlined in [25], by introducing two modes of transmission. This extension aims to account for the differing transmission and recovery rates exhibited by older individuals or those with underlying health conditions compared to other groups. Additionally, these individuals often have more complex medical needs and may require more intensive care. The model introduces separate compartments for exposed, infected, and asymptomatic individuals to capture these differences and provide a more detailed representation of disease dynamics. The nonlinear system that describes the dynamics of bi-modal epidemics is represented by:

$$\begin{aligned}
\dot{S}(t) &= \nu N - \frac{\beta_1 S I_1}{N} - \frac{\beta_2 S I_2}{N} - \mu^S S + \omega R(t) \\
\dot{\mathrm{E}}_1(\mathrm{t}) &= \frac{\beta_1 S I_1}{N} - (\kappa_1 + \mu_1^E) E_1 \\
\dot{E}_2(t) &= \frac{\beta_2 S I_2}{N} - (\kappa_2 + \mu_2^E) E_2 \\
\dot{I}_1(t) &= p_1 \kappa_1 E_1 - (\gamma_1 + \mu_1^I) I_1 \\
\dot{I}_2(t) &= p_2 \kappa_2 E_2 - (\gamma_2 + \mu_2^I) I_2 \\
\dot{A}_1(t) &= (1 - p_1) \kappa_1 E_1 - (\eta_1 + \mu_1^A) A_1 \\
\dot{A}_2(t) &= (1 - p_2) \kappa_2 E_2 - (\eta_2 + \mu_2^A) A_2 \\
\dot{R}(t) &= \gamma_1 (1 - \rho_1) I_1 + \gamma_2 (1 - \rho_2) I_2 \\
&\quad + \eta_1 A_1 + \eta_2 A_2 - (\mu^R + w) R
\end{aligned} \tag{1}$$

Therefore, this system includes eight positive state variables that represent the different compartments in the epidemiological model. The state variables and parameters are listed in Table 1.

TABLE I INTERPRETATION OF SYSTEM STATES

Variable	Description
S	Susceptible individuals
E_1	People with chronic illness who were exposed
E_2	People without chronic illness who were exposed
I_1	People with chronic illness who are infected
I_2	People without chronic illness who are infected
A_1	People with chronic illness who are asymptomatic
A_2	People without chronic illness who are asymptomatic
R	Recovered individuals

In this model, (S) denotes the number of individuals who are susceptible (i.e., those who are not yet infected), (E) represents the number of people exposed to infection (infected but not yet able to transmit the virus), and (I) includes infected individuals who are capable of transmitting the disease to susceptible individuals. (A) denotes the

number of asymptomatic carriers, while compartment (R) includes those who have recovered and possess immunity to the disease. Finally, (N) represents the total population size, expressed as: (i.e., $N(t) = S(t) + E_1(t) + E_2(t) + I_1(t) + I_2(t) + A_1(t) + A_2(t) + R(t)$).

The model equations describe how susceptible individuals (S) come into contact with infected individuals (I_i) at a rate of β_i, leading to their transition to the exposed group (E_i). Exposed individuals become infected at a rate of κ_i and are divided into two groups: those who develop symptoms and those who remain asymptomatic. A portion of the individuals who have been exposed enters the infected group, while the remainder transitions to the asymptomatic group, as described in [4] .Asymptomatic individuals (A_i) move from their group to the recovered category (R) at a rate of η_i. Infected individuals (I_i) also leave their group at a rate of γ_i, with a proportion of $(1-\rho_i)$ recovering and the remaining proportion (ρ_i) succumbing to the infection. The model takes into account the decreasing immunity of recovered individuals, using parameter ω to determine the average duration of immunity. After this period, individuals who have recovered transition back to the susceptible group. The symbols ν, and μ represents the birth rate and mortality rate from natural causes, respectively.

All the model parameters $(\beta_i, \kappa_i, p_i, \gamma_i, \eta_i, \omega_i, \nu)$, and μ assumed to be positive to accurately reflect real-world conditions. A conceptual flow diagram that visualizes the relationships among the dynamics of the model is shown in Fig. 1.

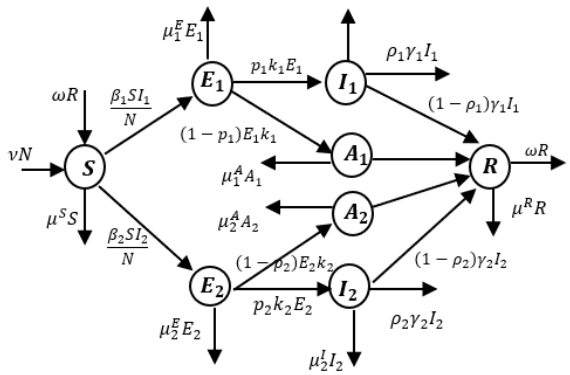


Fig. 1. Conceptual flow diagram of the two-group SEIAR model with death/birth rate.

The total population dynamics at time t can be calculated by summing all the equations in (1), leading to:

$$\dot{N}(t) = \nu N - \mu^S S - \mu_1^E E_1 - \mu_2^E E_2 - (\mu_1^I + \gamma_1\rho_1) I_1 - (\mu_2^I + \gamma_2\rho_2) I_2 - \mu^R R \quad (2)$$

We develop the epidemic model by incorporating parallel interventions, including vaccination, antiviral treatment, and social distancing strategies, as represented by the following system of differential equations:

$$\begin{aligned}
\dot{S}(t) &= -\frac{\beta_1 I_1 S}{N}(1 - sat(u_2)) \\
&\quad -\frac{\beta_2 I_2 S}{N}(1 - sat(u_3)) - \mu^S S + \nu N \\
&\quad +\omega R(t) - N sat(u_1) + d_S(t) \\
\dot{E}_1(t) &= \frac{\beta_1 S I_1}{N}\big(1 - \mathrm{sat}(u_2)\big) - (\kappa_1 + \mu_1^E) E_1 \\
&\quad +d_{E_1}(t) \\
\dot{E}_2(t) &= \frac{\beta_2 S I_2}{N}(1 - sat(u_3)) - (\kappa_2 + \mu_2^E) E_2 \\
&\quad +d_{E_2}(t) \\
\dot{I}_1(t) &= p_1 \kappa_1 E_1 - (\gamma_1 + \mu_1^I) I_1 - \mathrm{sat}(u_4) I_1 \\
&\quad +d_{I_1}(t) \\
\dot{I}_2(t) &= p_2 \kappa_2 E_2 - (\gamma_2 + \mu_2^I) I_2 - \mathrm{sat}(u_5) I_2 \\
&\quad +d_{I_2}(t) \\
\dot{A}_1(t) &= (1 - p_1)\kappa_1 E_1 - (\eta_1 + \mu_1^A) A_1 \\
&\quad +d_{A_1}(t) \\
\dot{A}_2(t) &= (1 - p_2)\kappa_2 E_2 - (\eta_2 + \mu_2^A) A_2 \\
&\quad +d_{A_2}(t) \\
\dot{R}(t) &= \gamma_1(1 - \rho_1) I_1 + \gamma_2(1 - \rho_2) I_2 \\
&\quad +\eta_1 A_1 + \eta_2 A_2 - (\mu^R + w) R \\
&\quad +sat(u_4) I_1 + sat(u_5) I_2 + N sat(u_1) \\
&\quad +d_R(t)
\end{aligned} \quad (3)$$

The equations include five control inputs, $(u_1(t), u_2(t), u_3(t), u_4(t))$, and $u_5(t)$ which are crucial for achieving the desired outcome. The control function $0 \le u_1(t) \le 1$ quantifies the rate at which the total population is vaccinated. Similarly, the control factors $0 \le u_2(t) \le 1$, and $0 \le u_3(t) \le 1$ effectively reduces the contact rate through social distancing measures. The control functions $0 \le u_4(t) \le 1$ and $0 \le u_5(t) \le 1$ measure the rate at which infectious individuals, both with and without comorbidities, receive treatment during each period, thereby aiding in recovery. The saturation function of the control inputs $(i.e., sat(u))$ is defined as follows:

$$sat\big(u(t)\big) = \begin{cases} sign\big(u(t)\big)u_M, & |u(t)| \ge u_M \\ u(t), & |u(t)| < u_M \end{cases} \quad (4)$$

where u_M represents the saturation limit of the input. The vector of perturbations caused by uncertainties and time-varying external disturbances, denoted as $d_i(t), i \in \{S, E_1, E_2, I_1, I_2, A_1, A_2, R\}$, plays a crucial role in enhancing the robustness and accuracy of the model. By considering various sources of uncertainties and disturbances, such as migration and travel patterns, changes in public health policies, and economic factors, the model can better capture the complexities and dynamics of the real world. This approach leads to more reliable predictions and improved decision-making capabilities. We assume that the upper bound of $d(t)$ is unknown. Our proposed control strategy aims to track desired descending reference signals for the state variables $S, E_1, E_2, I_1,$ and I_2. Consequently, the controller seeks to reduce the number of susceptible, exposed, and infected individuals to zero $(i.e., S \rightarrow$

$0, E_1 \to 0, E_2 \to 0, I_1 \to 0$ and $I_2 \to 0$) by monitoring specific situations and employing control inputs. In these scenarios, it is demonstrated that the other state variables are constrained and approach zero $(i.e., A_1, A_2 \to 0)$. As a result, the population removed by immunity asymptotically tracks the total population. $(i.e., R \to N)$.

A. Positivity and Boundedness of the Solution

For an epidemic model to be effective for its intended applications, it must yield positive and bounded solutions. Consequently, the solutions of system (1) must be constrained to remain positive and bounded in accordance with the given initial conditions:

$\big(S(0), E_1(0), E_2(0), I_1(0), I_2(0), A_1(0), A_2(0), R(0)\big) \in R_8^+$

Proposition 1. In the positive orthant of R_8^+, the system (1) must exhibit positivity and invariance.

Proof. When the value of (S) reaches zero at a time (t), all other state variables are also effectively reset to zero at that time. At time (t), this condition is expressed as:

$$\dot{S}(t)\big|_{S(t)=0} = \nu N + \omega R \geq 0$$

Due to the positivity of the model parameters, as well as the number of recovered individuals and the total population, (S) will only increase and will not decrease. Similarly, the remaining state variables also exhibit this behavior.

$$\dot{E}_1(t)\big|_{E_1(t)=0} = \frac{\beta_1 S I_1}{N} \geq 0$$
$$\dot{E}_2(t)\big|_{E_2(t)=0} = \frac{\beta_2 S I_2}{N} \geq 0$$
$$\dot{I}_1(t)\big|_{I_1(t)=0} = p_1 \kappa_1 E_1 \geq 0$$
$$\dot{I}_2(t)\big|_{I_2(t)=0} = p_2 \kappa_2 E_2 \geq 0$$
$$\dot{A}_1(t)\big|_{A_1(t)=0} = (1-p_1)\kappa_1 E_1 \geq 0$$
$$\dot{A}_2(t)\big|_{A_2(t)=0} = (1-p_2)\kappa_2 E_2 \geq 0$$
$$\dot{R}(t)\big|_{R(t)=0} = \gamma_1(1-\rho_1)I_1 + \gamma_2(1-\rho_2)I_2 + \eta_1 A_1 + \eta_2 A_2 \geq 0$$

As a result, in R_8^+, all of the state variables are nonnegative and form an invariant set for model (1).

Proposition 2. In the feasible region Γ, the system (1) is bounded.

$$\Gamma = \{(S, E_1, E_2, I_1, I_2, A_1, A_2, R) \in R_8^+ : 0 \leq S(t) + E_1(t) + E_2(t) + I_1(t) + I_2(t) + A_1(t) + A_2(t) + R(t) \leq \frac{\nu N}{\mu^*}\}$$

where $\mu^* = \min\{\mu^S, \mu_1^E, \mu_2^E, \mu_1^I + \gamma_1\rho_1, \mu_2^I + \gamma_2\rho_2, \mu^R\}$

Proof. The sum of all equations in the model (1) results in the following equation for the total population.

$$\begin{aligned}\dot{N}(t) &= \nu N - \mu^S S - \mu_1^E E_1 - \mu_2^E E_2 - \mu^R R \\ &\quad -(\mu_1^I + \gamma_1\rho_1)I_1 - (\mu_2^I + \gamma_2\rho_2)I_2 \\ &\leq \nu N - \mu^*(S + E_1 + E_2 + I_1 + I_2 + R)\end{aligned} \quad (5)$$

One can obtain from equation (5) that

$$N(t) \leq N(0)e^{-\mu^* t} + \frac{\nu N}{\mu^*}(1 - e^{-\mu^* t})$$
$$N(t) \leq \frac{\nu N}{\mu^*}, \quad if\ N(0) \leq \frac{\nu N}{\mu^*}$$

It can be verified that Γ is positively invariant with respect to (1).

B. The basic Reproduction number

In epidemic theory, the basic reproduction number, commonly denoted as R_0, is one of the most critical concepts due to its ability to predict the course of an epidemic. It represents the average number of secondary infections caused by a single infected individual during their infectious period [4] .The value of R_0 is instrumental in determining the stability of operating points [5]. If $R_0 < 1$, the disease-free equilibrium is locally asymptotically stable, indicating that the epidemic will self-eradicate. If $R_0 > 1$, the disease-free equilibrium is unstable, and there will always be a non-zero number of infectious individuals within the population. System (1) always has the disease-free equilibrium. To find this equilibrium, all infected variables must be set to zero $(i.e., E_1 = E_2 = I_1 = I_2 = A_1 = A_2 = 0)$ and the remaining variables are solved accordingly. Thus, the equilibrium of the population in the absence of disease is obtained as follows:

$$Q_0 = (\tfrac{\nu N}{\mu^S}, 0, 0, 0, 0, 0, 0, 0)$$

One common approach to calculating R_0 is the next-generation matrix method [4]. This method involves constructing a matrix that represents the average number of new infections generated by an infected individual across each compartment of the epidemiological model. Let $\chi_1(t) = [E_1\ I_1\ A_1]^T$, and $\chi_2(t) = [E_2\ I_2\ A_2]^T$.

Then, the dynamics of the system can be described by the following equations:

$$\dot{\chi}_i = \mathcal{F}_i(\chi) - \mathcal{V}_i(\chi) \quad (6)$$

Here, $\mathcal{F}_i(\chi)$ represents the rate of appearance of new individuals in group (i), while $\mathcal{V}_i(\chi)$ signifies the difference between the rate at which individuals enter group (i) and the rate at which they leave it. For individuals with underlying health conditions, in the virus-free environment Q_0, The non-negative matrices $F = = \left[\frac{\partial \mathcal{F}_i}{\partial x_j}\right]$ and $V = \left[\frac{\partial \mathcal{V}_i}{\partial x_j}\right]$ are defined as follows:

$$F_1 = \begin{bmatrix} 0 & \frac{\beta_1 S}{N} & 0 \\ 0 & 0 & 0 \\ 0 & 0 & 0 \end{bmatrix}$$

$$V_1 = \begin{bmatrix} (\kappa_1 + \mu_1^E) & 0 & 0 \\ -p_1\kappa_1 & (\gamma_1 + \mu_1^I) & 0 \\ -(1-p_1)k_1 & 0 & (\eta_1 + \mu_1^A) \end{bmatrix}$$

Set $R_0^1 = \Omega(\mathcal{F}_1 {\mathcal{V}_1}^{-1})$, Where $\Omega(\mathrm{A})$ denotes the spectral radius of matrix A. Thus, the basic reproduction ratio for individuals suffering from serious disease is given by:

$$R_0^1 = \frac{\beta_1 p_1 k_1 \nu}{\mu^s(k_1 + \mu_1^E)(\gamma_1 + \mu_1^I)} \quad (7)$$

Similarly, for individuals with comorbidities, the basic reproduction number is given by

$$R_0^2 = \frac{\beta_2 p_2 k_2 \nu}{\mu^s(k_2 + \mu_2^E)(\gamma_2 + \mu_2^I)} \quad (8)$$

Hence, the basic reproduction ratio of the system (1) is given by [5].

$R_0 = max\{ R_0^1, R_0^2\}$

III. Design of Robust Controller

A. System Description and Preliminaries

Consider the following class of MIMO continuous-time nonlinear plants:

$$\dot{x}(t) = f\big(x(t)\big) + \sum_{j=1}^{m} g_j(x(t))sat(u_j(t)) + d(t),$$
$$y_i(t) = h_i\big(x(t)\big),\ i = j = 1,2,\cdots,m \quad (9)$$

where $y(t) \in \mathbb{R}^m, u(t) \in \mathbb{R}^m$, and $x(t) \in \mathbb{R}^n$ represent the output signal vector, the input signal vector, and the system's state vector, respectively. The term $f\big(x(t)\big) = \theta_f f_0\big(x(t)\big)$ denotes a smooth vector field, while $g(x(t)) = \theta_g g_0\big(x(t)\big)$ represents a smooth $m \times m$ nonlinear matrix. Here, θ_f and θ_g account for model uncertainties. $d(t)$ denotes an external disturbance with unknown bound. The control objective is to design a robust control scheme that ensures the outputs $y_i(t)$ track the desired trajectory $y_{d_i}(t)$. Tracking errors must remain within specified constraints while ensuring that all closed-loop signals are both bounded and positive.

B. Backstepping Control

Backstepping is a recursive design technique used to asymptotically stabilize controllers for systems in strict feedback form [19] .To design an appropriate backstepping controller, it is essential to derive the strict feedback form of the control system [26]. If the nonlinear system is not in strict feedback form, methods such as input-output linearization or alternative techniques can be employed to transform the system into the desired standard form. This transformation allows for the application of backstepping design techniques, facilitating the development of an effective controller for the nonlinear system. Assume that the system (9) is transformed into the following parametric strict-feedback system with zero dynamics via a diffeomorphism $[\psi^T, \eta^T]^T = \Phi(x)$ as follows [20]:

$$\dot{\eta} = q(\eta, \psi) \quad (10)$$

$$\dot{\psi}_{i,k} = \psi_{i,k+1},\ 1 \le k \le r_i - 1, 1 \le i \le m$$
$$\dot{\psi}_{i,r_i} = \theta_{b_i} b_i(\eta,\psi) + \sum_{j=1}^{m} \theta_{a_{ij}} a_{ij}(\eta,\psi) sat\big(u_j\big) + d_i(t), 1 \le j \le \mathrm{m} \quad (11)$$

Where $\eta(t) = [\eta_{r+1}(t)\ \eta_{r+2}(t)\ \cdots\ \eta_n(t)]^T$, $q(\eta,\psi)$, and $b_i(\eta,\psi) = L_f^{r_i} h_i(x)$ are known smooth vector functions. The term $a_{ij}(\eta,\psi) = L_{g_j} L_f^{r_i - 1} h_i(x)$ represents $(i,j) - th$ element of a known non-singular $m \times m$ matrix $\mathrm{A}(\eta,\psi)$, defined for all $[\psi^T, \eta^T]^T \in \mathbb{R}^n$. Here, θ_{a_i} and θ_{b_i} are vectors of unknown constant parameters. The integer r_i denotes the smallest relative degree of the $i - th$ with respect to any of the m inputs, and $r = r_1 + r_2 + \cdots + r_m$ is defined as the sum of individual relative degrees.

The relationship between the applied control $sat(u_j(t))$, and the control input $u_j(t)$ exhibits a sharp discontinuity when the absolute value of $u_j(t)$ reaches the saturation level u_{M_j}. This discontinuity presents a challenge for the direct application of the backstepping technique. To address this issue, we approximate the saturation function with a smooth function. A commonly used approximation is the hyperbolic tangent function, defined as follows [16]:

$$g(u_i) = u_{M_i} \tanh\left(\frac{u_i}{u_{M_i}}\right) = u_{M_i} \frac{e^{\frac{u_i}{u_{M_i}}} - e^{-\frac{u_i}{u_{M_i}}}}{e^{\frac{u_i}{u_{M_i}}} + e^{-\frac{u_i}{u_{M_i}}}} \quad (12)$$

Then $sat(u_j(t))$ in (11) can be expressed as follows

$$sat\left(u_j(t)\right) = g\big(u_j\big) + d\big(u_j\big) = u_{M_j} \tanh\left(\frac{u_j}{u_{M_j}}\right) + d\big(u_j\big) \quad (13)$$

where $d\big(u_j\big) = sat\big(u_j\big) - g(u_j)$ is a bounded function, and its bound can be obtained as

$$\big|d\big(u_j\big)\big| = \big|sat\big(u_j\big) - g\big(u_j\big)\big| \le u_{M_j}(1 - \tanh(1)) = 0.2785 u_{M_j} \quad (14)$$

So, the equations (10) and (11) can be written as

$$\dot{\eta} = q(\eta,\psi) \quad (15)$$

$$\dot{\psi}_{i,k} = \psi_{i,k+1},\ \ 1 \le k \le r_i - 1,\ \ 1 \le i,j \le m \quad (16)$$

$$\dot{\psi}_{i,r_i} = \theta_{b_i} b_i(\eta,\psi) + \sum_{j=1}^{m} \theta_{a_{ij}} a_{ij}(\eta,\psi) g\big(u_j\big) + \Delta d_i(t)$$

where $\Delta d_i(t) = \sum_{j=1}^{m} \theta_{a_{ij}} a_{ij}(\eta,\psi) d\big(u_j\big) + d_i(t)$

Assumption 1. The nonlinear plant (9) is feedback linearizable without saturation.

Assumption 2. The desired trajectory y_{d_i} and its $r_i -$ th derivatives are known, bounded, and piecewise continuous.

Assumption3. The zero dynamics of the system $\dot{\eta} = q(\eta,\psi)$ are input-to-state stable.

Definition 1. A function N(s) is considered a Nussbaum-type function when it possesses the properties listed [27].

$$\lim_{s\to\pm\infty}\sup\frac{1}{s}\int_0^s N(\mathcal{X})d\mathcal{X}=\infty, \tag{17}$$

$$\lim_{s\to\pm\infty}\inf\frac{1}{s}\int_0^s N(\mathcal{X})d\mathcal{X}=-\infty \tag{18}$$

According to the definition, Nussbaum functions must exhibit both infinite gains and infinite switching frequencies. Examples of such functions include $\mathcal{X}^2\cos(\mathcal{X})$, $\mathcal{X}^2\sin(\mathcal{X})$, $\mathrm{e}^{\mathcal{X}^2}\cos\left(\frac{\pi}{2}\mathcal{X}\right)$,and $\mathrm{e}^{\mathcal{X}^2}\sin\left(\frac{\pi}{2}\mathcal{X}\right)$. The selection of this particular Nussbaum functions is based on its advantageous properties:

1. Its infinite oscillatory nature ensures adaptive control gains capable of addressing unknown input saturation levels.
2. Its smoothness and bounded derivative allow for seamless integration into the backstepping design while preserving the validity of the Lyapunov-based stability analysis.

This paper utilizes the Nussbaum function $\mathcal{X}^2\cos(\mathcal{X})$. The following lemma presents the property of Nussbaum functions.

Lemma 1 [28, 29]**:** Smooth functions $V(.)$ and $\mathcal{X}(.)$ are defined on $[0,t_f)$ with $V(t)\geq 0,\forall t\in[0,t_f)$, and $\mathcal{N}(\mathcal{X})$ is a Nussbaum gain function. If the inequality is satisfied, $V(.)$ and $\mathcal{X}(.)$ must be limited on the interval $[0,t_f)$.

$$\begin{aligned}V\leq V(0)e^{-Ct}+\frac{M}{C}(1-e^{-Ct})\\ +\frac{e^{-Ct}}{\gamma_{\mathcal{X}}}\int_0^t(\xi\mathcal{N}(\mathcal{X})\dot{\mathcal{X}}-\dot{\mathcal{X}})e^{C\tau}\,d\tau\end{aligned} \tag{19}$$

where $C>0, M>0, \gamma_{\mathcal{X}}>0$ are constants, and ξ is a positive variable.

C. Design of adaptive backstepping sliding mode controller and stability analysis

This section combines the backstepping method with adaptive sliding mode control to design an adaptive backstepping-sliding-mode controller, ensuring robust control for uncertain systems. The backstepping technique formulates a virtual control law to achieve asymptotic convergence of the tracking error to zero. Simultaneously, adaptive sliding mode control is employed to develop a robust control law that compensates for system uncertainties and disturbances. To enhance performance, integral action is incorporated into the backstepping control, mitigating steady-state bias and reducing rise time. For the system described in equations (10) and (11), integral backstepping is implemented by introducing the integral term of the tracking error, $\int_0^t\left(\psi_i(\tau)-\psi_{d_i}(\tau)\right)d\tau$ at the initial stage of backstepping. This approach maintains the strict feedback form of the system, while the relative degree of each output vector is elevated to r_i+1, necessitating r_i+1 steps of backstepping.

To address the challenge of input saturation, the control scheme incorporates a novel auxiliary design system alongside Nussbaum gain functions. Input saturation, often caused by actuator limitations, introduces significant nonlinearities that can destabilize the system. The Nussbaum function, with its oscillatory behavior and unbounded growth properties, dynamically adjusts control gains to counteract these nonlinearities without requiring precise knowledge of the saturation limits.

Additionally, the Nussbaum function ensures the boundedness and positivity of system states, which is essential in scenarios such as epidemic models, where negative states are not physically meaningful. By leveraging its adaptive characteristics, it enables accurate trajectory tracking even in the presence of disturbances or saturation effects. The auxiliary design system complements the control strategy by creating a control law that effectively manages input saturation, while the Nussbaum gain functions enhance the overall robustness of the system, ensuring precise tracking of the desired trajectory.

$$\begin{aligned}&\dot{\psi}_{i,1}=\psi_{i,2}-\psi_{d_i}\\&\dot{\psi}_{i,2}=\psi_{i,3}\\&\vdots\\&\dot{\psi}_{i,r_i+1}=\theta_{b_i}b_i(\eta,\psi)\\&\qquad+\sum_{j=1}^{m}\theta_{a_{ij}}a_{ij}(\eta,\psi)g(u_j)+\Delta d_i(t),\\&\dot{\eta}=q(\eta,\psi)\\&y_i=\psi_{i,2},\qquad i=j=1,2,\cdots,m\end{aligned} \tag{20}$$

$$\dot{u}_j=-k_ju_j+w_j \tag{21}$$

where k_j are positive constants and w_j are auxiliary signals to be designed in the backstepping approach. Consequently, the design of the control law transitions to the design of w_j. It is clear that all functions in equations (20) and (21) are continuous, allowing for the successful application of the backstepping technique. The design involves a procedure of r_i+2 steps for each subsystem, wherein each subsystem has a relative degree of order r_i. At each step, an error variable z_i is defined, and a stabilizing function α_i constructed to stabilize the $i-th$ output with respect to a Lyapunov function V_i. The state feedback control is provided in the final stage. The structure of the closed-loop system is illustrated in Fig. 2.

Remark 1: The augmented systems (20), and (21) differ from those examined using the conventional backstepping method. This distinction arises because $\dot{\psi}_{r_i+1}$ is directly related to the nonlinear function $g(u_j)$ rather than just u_j.

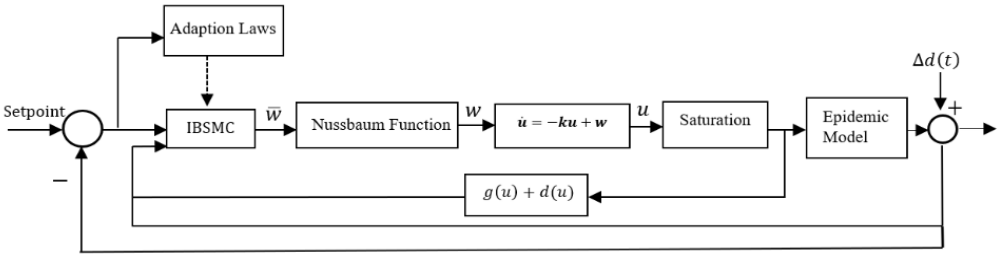


Fig. 2. Schematic diagram of adaptive backstepping sliding mode control strategy

As a result, the term $(\frac{\partial g}{\partial u_j})\dot{u}_j$ is introduced instead of $\dot{u}_j$, marking a departure from previous backstepping strategies. To address this issue, a Nussbaum function is employed.

Remark 2: System (20) contains the function $g(u_j)$, which acts as a control input for systems studied with backstepping techniques. Designing the control signal u_j without using a direct method is challenging in our current scenario. To address this issue, we intentionally include (21) to generate a reliable control signal u_j by establishing an auxiliary control signal w_i during the last step $r_i + 2$ of the backstepping procedure.

In the standard backstepping method for tracking problems, a coordinate transformation is applied to the $i-th$ output as follows:

$$z_{i,1} = \psi_{i,1} = \int_0^t (\psi_{i,2} - \psi_{d_i}) d\tau \tag{22}$$

$$z_{i,k} = \psi_{i,k} - \psi_{d_i}^{(k-2)} - \alpha_{i,k-1}, k = 2, \cdots, r_i + 1 \tag{23}$$

$$z_{i,r_i+2} = g(u_i) - \alpha_{i,r_i+1}\,, \tag{24}$$

where z_k and α_{k-1} represent the tracking error and the virtual control input that needs to be determined at the $k-th$ step, the introduction of variable z_{i,r_i+2} results from including the new state variable u_i. The design procedure for adaptive backstepping sliding mode control of a MIMO system, adhering to assumptions 1-3, comprises $r_i + 2$ steps for $i-th$ output, as follows:

Step k $(k = 1,2, \cdots, r_i)$: We define the virtual control law α_k for $i-th$ output as follows:

$$\alpha_{i,1}(z_{i,1}) = -c_{i,1} z_{i,1} \tag{25}$$

$$\alpha_{i,k} = -c_{i,k} z_{i,k} - z_{i,k-1} + \sum_{j=1}^{k-1} \left(\frac{\partial \alpha_{i,k-1}}{\partial \psi_{i,j}} \psi_{i,j+1} + \frac{\partial \alpha_{i,k-1}}{\partial \psi_{d_i}^{(j-1)}} \psi_{d_i}^{(j)}\right) \tag{26}$$

where $c_{i,k}$ are positive design parameters. The Lyapunov function is proposed as follows:

$$V_{i,k} = \sum_{j=1}^{k} \frac{1}{2} z_{i,j}^2 \tag{27}$$

Then, the derivative of $V_{i,k}$, along with equations (22) and (23), is given by:

$$\dot{V}_{i,k}(z_{i,1}, z_{i,2}, \cdots, z_{i,k}) = -\sum_{j=1}^{k} c_{i,j} z_{i,j}^2 + z_{i,k} z_{i,k+1} \tag{28}$$

Step k $= r_i + 1$: The time derivative of the tracking error $z_{i,k}$ from equations (20) and (23) is derived as follows:

$$\begin{aligned} \dot{z}_{i,k} &= \dot{\psi}_{i,k} - \psi_{d_i}^{(k-1)} - \dot{\alpha}_{i,k-1} \\ &= \theta_{b_i} b_i(\eta, \psi) + \theta_{a_i} a_i(\eta, \psi)(z_{i,k+1} \\ &\quad + \alpha_{i,k}) + \Delta d_i - \psi_{d_i}^{(k-1)} - \dot{\alpha}_{i,k-1} \end{aligned} \tag{29}$$

where $g(u_i) = z_{i,k+1} + \alpha_{i,k}$ has been utilized. We design the virtual control law $\alpha_{i,k}$ as follows:

$$\begin{aligned} \alpha_{i,k} = (\hat{\theta}_{a_i} a_i(\eta, \psi))^{-1} [&-c_{i,k} z_{i,k} - z_{i,k-1} \\ &- \hat{\theta}_{b_i} b_i(\eta, \psi) + \psi_{d_i}^{(k-1)} - \Delta d_i(t) \\ &+ \dot{\alpha}_{i,k-1}] \end{aligned} \tag{30}$$

It should be noted that $\hat{\theta}_{a_i}$ and $\hat{\theta}_{b_i}$ are the estimated values of the uncertain system parameters as described in equation (20), and these estimates have bounded errors relative to their corresponding unknown true values θ_{a_i} and θ_{b_i}, respectively. To effectively estimate the uncertainties in the θ_i vectors, the proposed control approach incorporates an adaptive estimation mechanism. This mechanism employs parameter adaptation, allowing the controller to continuously update its estimates of the uncertain parameters based on observed system outputs. Incorporating a switching term into α_k with $s_i = z_{i,k}$ as the sliding surface helps maintain robust performance despite uncertainties and external disturbances. Therefore, the virtual control $\alpha_{i,k}$ is structured in this manner.

$$\begin{aligned} \alpha_{i,k} = (\hat{\theta}_{a_i} a_i(\eta, \psi))^{-1} [&-c_{i,k} z_k - z_{i,k-1} \\ &- \hat{\theta}_{b_i} b_i(\eta, \psi) + \psi_{d_i}^{(k-1)} - \hat{\gamma}_{i,k} sgn(z_{i,k}) \\ &+ \dot{\alpha}_{i,k-1}] \end{aligned} \tag{31}$$

where $\hat{\gamma}_{i,k}$ represents the robust gains of the proposed controller, which are updated using adaptation laws to ensure stability in the presence of modeling uncertainties. Through adaptive estimation, the controller is capable of learning and adapting to the uncertainties in the θ vectors in real time. This enables the controller to effectively handle modelling uncertainties and achieve robust performance despite changing or unknown system dynamics. The discontinuity of the $sign(.)$ function introduces non-differentiability issues,

complicating the subsequent design procedure. To overcome this challenge and obtain a smooth control signal, the hyperbolic tangent function can replace the discontinuous sign function in (31). Ultimately, the stabilizing function $\alpha_{i,k}$ is verified as the follows:

$$\begin{aligned}\alpha_{i,k} = (\hat{\theta}_{a_i} a_i(\eta,\psi))^{-1}[&-c_{i,k} z_{i,k} - z_{i,k-1} \\ &-\hat{\theta}_{b_i} b_i(\eta,\psi) + \psi_{d_i}^{(k-1)} \\ &-\hat{\gamma}_{i,k} tanh\left(\frac{z_{i,k}}{\varepsilon_i}\right) + \dot{\alpha}_{i,k-1}]\end{aligned} \tag{32}$$

$\varepsilon_i > 0$ is the boundary layer coefficient. By substituting $\Psi_i = -c_{i,k} z_{i,k} - z_{i,k-1} + \psi_{d_i}^{(k-1)} + \dot{\alpha}_{i,k-1}$, it can be expressed as:

$$\begin{aligned}\alpha_{i,k} = (\hat{\theta}_{a_i} a_i(\eta,\psi))^{-1}[&\Psi_i - \\ &\hat{\gamma}_{i,k} tanh\left(\tfrac{z_{i,k}}{\varepsilon_i}\right) - \hat{\theta}_{b_i} b_i(\eta,\psi)]\end{aligned} \tag{33}$$

By introducing the regressor matrices Y_i, and the parameter vectors θ_i for (33), the parameters with uncertainties in the θ_i vectors are separated from the known dynamic variables in the Y_k matrices. This relationship can be expressed as $\alpha_{i,k} = Y_i \hat{\theta}_i$, where

$$\begin{aligned}Y_i = &\\ &[a_i(\eta,\psi)^{-1}(\Psi_i - \hat{\gamma}_{i,k} tanh\left(\frac{z_{i,k}}{\varepsilon_i}\right)) \\ &, -a_i(\eta,\psi)^{-1} b_i(\eta,\psi)] \\ \theta_i = &[\frac{1}{\theta_{a_i}} \quad \frac{\theta_{b_i}}{\theta_{a_i}}]^T\end{aligned} \tag{34}$$

By substituting the nonlinear virtual control laws from (33) into the dynamics given by (20), the closed-loop system using the proposed robust adaptive controller is obtained as follows:

$$\begin{aligned}&(\theta_{a_i} a_i(\eta,\psi))^{-1}\dot{\psi}_{i,k} - \Psi_i \\ &+(\hat{\theta}_{a_i} a_i(\eta,\psi))^{-1}\hat{\gamma}_{i,k} tanh\left(\frac{z_{i,k}}{\varepsilon_i}\right) \\ &= \left[\frac{\theta_{b_i}}{\theta_{a_i}} - \frac{\hat{\theta}_{b_i}}{\hat{\theta}_{a_i}}\right]\frac{b_i(\eta,\psi)}{a_i(\eta,\psi)}\end{aligned} \tag{35}$$

Thus, after employment of the regressor matrices Y_i and the parameter vectors θ_i, the above equations can be rewritten as follows:

$$\begin{aligned}\dot{z}_{i,k} = &-c_{i,k} z_{i,k} + a_i(\eta,\psi)\theta_{a_i} Y_i \tilde{\theta}_i \\ &-\hat{\gamma}_{i,k} tanh\left(\frac{z_{i,k}}{\varepsilon_i}\right)\end{aligned} \tag{36}$$

Where $\tilde{\theta}_i = \theta_i - \hat{\theta}_i$ represents the bounded error vector of the model parameters estimation. As the state variables and the estimation errors of unknown parameters $\tilde{\theta}_i$ are bounded, there exist positive unknown constant $\mu_{i,1}$, and $\mu_{i,2}$ such that

$$\left| a_i(\eta,\psi)\theta_{a_i} Y_i \tilde{\theta}_i \right| < \mu_{i,1} \tag{37}$$

$$\left| (\frac{\partial \alpha_{i,k}}{\partial \psi_{i,k}})[b_i(\eta,\psi)(\theta_{b_i} - \hat{\theta}_{b_i}) + a_i(\eta,\psi)(\theta_{a_i} - \hat{\theta}_{a_i}) g(u_i) \right| < \mu_{i,2} \tag{38}$$

To achieve robustness against modeling uncertainties, the parameter updates laws for updating the robust gains $\hat{\gamma}_{\mathrm{i,k}}$, and $\hat{\gamma}_{\mathrm{i,k+1}}$ are designed as follows:

$$\frac{d\hat{\gamma}_{i,k}(t)}{dt} = \Gamma_{i.k}\left|z_{i,k}(t)\right|, \qquad \hat{\gamma}_{i,k}(0) > 0 \tag{39}$$

$$\frac{d\hat{\gamma}_{i,k+1}(\mathrm{t})}{dt} = \Gamma_{i,k+1}\left|z_{i,k+1}(t)\right|, \hat{\gamma}_{i,k+1}(0) > 0 \tag{40}$$

The positive constant parameters $\Gamma_{i,k}$, and $\Gamma_{\mathrm{i,k+1}}$ determine the rate at which the tracking errors are updated. Additionally, $\hat{\gamma}_{\mathrm{i,k}}(0)$, and $\hat{\gamma}_{i,k+1}(0)$ represent the initial positive values of the robust gains at $t = 0$. By employing adaptive estimation, the controller can adjust to the uncertainties in the θ_i vectors in real time. This capability enables the controller to effectively manage modeling uncertainties and achieve robust performance in the presence of changing or unknown system dynamics.

Now, the Lyapunov theorem is utilized to ensure the stability and robustness of the closed-loop system, as well as tracking convergence to the desired outputs. We define a new candidate Lyapunov function as follows:

$$\begin{aligned}&V_{i,k}(z_{i,1}, z_{i,2}, \cdots, z_{i,k}) \\ &= V_{i,k-1} + \frac{1}{2} z_{i,k}^2 + \frac{1}{2\Gamma_{i,k}} (\hat{\gamma}_{i,k} - \mu_{i,1})^2 \geq 0\end{aligned} \tag{41}$$

That its time-derivative, along with equations (28) and (36), is given by:

$$\begin{aligned}\dot{V}_{i,k} &= \dot{V}_{i,k-1} + z_{i,k}\dot{z}_{i,k} + \left|z_{i,k}\right|(\hat{\gamma}_{i,k} - \mu_{i,1}) \\ &= -\sum_{j=1}^{k-1} c_{i,j} z_{i,j}^2 + z_{i,k-1} z_{i,k} \\ &\quad + z_{i,k}[-c_{i,k} z_{i,k} + a_i(\eta,\psi)\theta_{a_i} Y_i \tilde{\theta}_i \\ &\quad - \hat{\gamma}_{i,k} tanh\left(\frac{z_{i,k}}{\varepsilon_i}\right)] + \left|z_{i,k}\right|(\hat{\gamma}_{i,k} - \mu_{i,1}) \\ &= -\sum_{j=1}^{k} c_{i,j} z_{i,j}^2 + z_{i,k-1} z_{i,k} \\ &\quad + z_{i,k} a_i(\eta,\psi)\theta_{a_i} Y_i \tilde{\theta}_i \\ &\quad - z_{i,k}\hat{\gamma}_{i,k} tanh\left(\tfrac{z_{i,k}}{\varepsilon_i}\right) + \left|z_{i,k}\right|\hat{\gamma}_{i,k} \\ &\quad - \left|z_{i,k}\right|\mu_{i,1}\end{aligned} \tag{42}$$

According to the equation (37), it can be expressed as:

$$\begin{aligned}\dot{V}_{i,k} &\leq -\sum_{j=1}^{k} c_{i,j} z_{i,j}^2 + z_{i,k-1} z_{i,k} + z_{i,k}\mu_{i,1} \\ &\quad - z_{i,k}\hat{\gamma}_{i,k} tanh\left(\frac{z_{i,k}}{\varepsilon_i}\right) + \left|z_{i,k}\right|\hat{\gamma}_{i,k} \\ &\quad - \left|z_{i,k}\right|\mu_{i,1} \\ &\leq -\textstyle\sum_{j=1}^{k} c_{i,j} z_{i,j}^2 + z_{i,k-1} z_{i,k} \\ &\quad - z_{i,k}\hat{\gamma}_{i,k} tanh\left(\frac{z_{i,k}}{\varepsilon_i}\right) + \left|z_{i,k}\right|\hat{\gamma}_{i,k}\end{aligned} \tag{43}$$

It is important to note that the following inequality holds true for all values of $\varepsilon > 0$ [13].

$$0 \le |z_{i,k}| - z_{i,k}\tanh\left(\frac{z_{i,k}}{\varepsilon_i}\right) \le c\varepsilon_i, \quad (44)$$

$$c = 0.2785$$

After some arrangement, the following inequality can be obtained:

$$\dot{V}_{i,k} \le -\sum_{j=1}^{k} c_{i,j} z_{i,j}^2 + z_{i,k-1}z_{i,k} + \hat{\gamma}_{i,k}\, c\varepsilon_i \quad (45)$$

Step $k+1$: From (20), (21), and (24), we obtain

$$\begin{aligned}\dot{z}_{i,k+1} = {} & \frac{\partial g}{\partial u_i}(-k_i u_i + w_i) \\ & -\frac{\partial \alpha_{i,k}}{\partial \psi_{i,k}}(\theta_{b_i} b_i(\eta,\psi) - \Upsilon_i \\ & + \theta_{a_i} a_i(\eta,\psi) g(u) + \Delta d_i(t)) \\ & -\frac{\partial \alpha_{i,k}}{\partial \hat{\gamma}_{i,k}}\Gamma_{i,k}|z_{i,k}|\end{aligned} \quad (46)$$

$$\Upsilon_i = \sum_{j=1}^{k-1}\frac{\partial \alpha_{i,k}}{\partial \psi_{i,j}}\psi_{i,j+1} + \sum_{j=1}^{k}\frac{\partial \alpha_{i,k}}{\partial y_{d_i}^{(j-1)}}\psi_d^{(j)} \quad (47)$$

Note that $\frac{\partial g}{\partial u}$ is a variable quantity, which adds complexity to the design and analysis procedures. To address this challenge, we introduce the Nussbaum function $N(\chi)$ as follows:

$$\mathcal{N}(\mathcal{X}) = \mathcal{X}^2\cos(\mathcal{X}) \quad (48)$$

A design for the backstepping control law for w_i is formulated in the following manner

$$w_i = \mathcal{N}(\mathcal{X}_i)\bar{w}_i \quad (49)$$

$$\dot{\mathcal{X}}_i = \gamma_{\mathcal{X}_i} z_{i,k+1}\bar{w}_i \quad (50)$$

$$\begin{aligned}\bar{w}_i = {} & -c_{i,k+1}z_{i,k+1} + \Upsilon_i + \frac{\partial \alpha_{i,k}}{\partial \hat{\gamma}_{i,k}}\Gamma_{i,k}|z_{i,k}| \\ & + \frac{\partial \alpha_{i,k}}{\partial \psi_{i,k}}(\hat{\theta}_{b_i} b_i(\eta,\psi) - z_{i,k} \\ & + \hat{\theta}_{a_i} a_i(\eta,\psi) g(u)) + \frac{\partial g}{\partial u_i} k_i u_i \\ & -\mathcal{L}_i\left(\frac{\partial \alpha_{i,k}}{\partial \psi_{i,k}}\right)^2 z_{i,k+1} \\ & -\hat{\gamma}_{i,k+1}\tanh\left(\frac{z_{i,k+1}}{\varepsilon_i}\right)\end{aligned} \quad (51)$$

The coefficients $c_{i,k+1}, \mathcal{L}_i$, and $\gamma_{\mathcal{X}_i}$ are positive design parameters. To analyze the designed system, we now consider an augmented positive Lyapunov function given by:

$$\begin{aligned}V_{i,k+1}(z_{i,1}, z_{i,2}, \cdots, z_{i,k+1}) = {} & V_{i,k} + \frac{1}{2}z_{i,k+1}^2 \\ & + \frac{1}{2\Gamma_{i,k+1}}(\hat{\gamma}_{i,k+1} - \mu_{i,2})^2\end{aligned} \quad (52)$$

The Lyapunov function is positive definite. The derivative of $V_{i,k+1}$ is obtained as follows:

$$\begin{aligned}\dot{V}_{i,k+1} = {} & -\sum_{j=1}^{k} c_{i,j} z_{i,j}^2 + z_{i,k}z_{i,k+1} + \hat{\gamma}_{i,k}\, c\varepsilon_i \\ & + z_{i,k+1}(\dot{z}_{i,k+1} + \bar{w}_i - \bar{w}_i) \\ & + |z_{i,k+1}|(\hat{\gamma}_{i,k+1} - \mu_{i,2})\end{aligned} \quad (53)$$

Substituting equation (51) into (53) and using the adaptation law from (40) yields:

$$\begin{aligned}\dot{V}_{i,k+1} = {} & -\sum_{j=1}^{k} c_{i,j} z_{i,j}^2 + z_{i,k}z_{i,k+1} + \hat{\gamma}_{i,k}\, c\varepsilon_i \\ & -z_{i,k+1}\bar{w}_i + |z_{i,k+1}|(\hat{\gamma}_{i,k} - \mu_{i,2}) \\ & + z_{i,k+1}\Big(\frac{\partial g}{\partial u_i}w_i - c_{i,k+1}z_{i,k+1} - z_{i,k} \\ & -\frac{\partial \alpha_{i,k}}{\partial \psi i_{,k}}\Delta d_i - \mathcal{L}_i\left(\frac{\partial \alpha_{i,k}}{\partial \psi_{i,k}}\right)^2 z_{i,k+1} \\ & -\frac{\partial \alpha_{i,k}}{\partial \psi_{i,k}} b_i(\eta,\psi)(\theta_{b_i} - \hat{\theta}_{b_i}) \\ & -\frac{\partial \alpha_{i,k}}{\partial \psi_{i,k}} a_i(\eta,\psi)(\theta_{a_i} - \hat{\theta}_{a_i}) g(u) \\ & -\hat{\gamma}_{i,k+1}\tanh\left(\frac{z_{i,k+1}}{\varepsilon_i}\right)\Big)\end{aligned} \quad (54)$$

According to equation (38), it can be expressed as follows:

$$\begin{aligned}\dot{V}_{i,k+1} \le {} & -\sum_{j=1}^{k} c_{i,j} z_{i,j}^2 + z_{i,k}z_{i,k+1} + \hat{\gamma}_{i,k}\, c\varepsilon_i \\ & -z_{i,k+1}\bar{w}_i + |z_{i,k+1}|(\hat{\gamma}_{i,k+1} - \mu_{i,2}) \\ & + z_{i,k+1}\Big(\frac{\partial g}{\partial u_i}w_i - c_{i,k+1}z_{i,k+1} - z_{i,k} - \frac{\partial \alpha_{i,k}}{\partial \psi_{i,k}}\Delta d_i \\ & -\mu_{i,2} - \mathcal{L}_i\left(\frac{\partial \alpha_{i,k}}{\partial \psi_{i,k}}\right)^2 z_{i,k+1} - \hat{\gamma}_{i,k+1}\tanh\left(\frac{z_{i,k+1}}{\varepsilon_i}\right)\Big) \\ \le {} & -\sum_{j=1}^{k+1} c_{i,j} z_{i,j}^2 + \hat{\gamma}_{i,k}\, c\varepsilon_i - z_{i,k+1}\bar{w}_i + z_{i,k+1}\frac{\partial g}{\partial u_i}w_i \\ & -z_{ik+1}\frac{\partial \alpha_{i,k}}{\partial \psi_{i,k}}\Delta \mathrm{d}_i - \mathcal{L}_i\left(\frac{\partial \alpha_{i,k}}{\partial \psi_{i,k}}\right)^2 z_{i,k+1}^2 \\ & + |z_{i,k+1}|\hat{\gamma}_{i,k+1} - \hat{\gamma}_{i,k+1}\, z_{i,k+1}\tanh\left(\frac{z_{i,k+1}}{\varepsilon_i}\right)\end{aligned} \quad (55)$$

By substituting equations (49) and (44) and utilizing the inequality $ab \le \frac{a^2}{2} + \frac{b^2}{2}$, one can write

$$\begin{aligned}\dot{V}_{i,k+1} \le {} & -\textstyle\sum_{j=1}^{k+1} c_{i,j} z_{i,j}^2 + \hat{\gamma}_{i,k} c\varepsilon_i + \hat{\gamma}_{i,k+1} c\varepsilon_i \\ & + z_{i,k+1}\frac{\partial g}{\partial u_i}(\mathcal{N}(\mathcal{X}_i) - 1)\bar{w}_i + \frac{1}{4\mathcal{L}_i}D_i^2\end{aligned} \quad (56)$$

where D_i is a constant which denotes the bound of $\Delta d_i(t)$ and may not be available. Substituting equation (50) into equation (56) yields:

$$\begin{aligned}\dot{V}_{i,k+1} \le {} & -CV_{i,k+1} + M_i \\ & + \frac{1}{\gamma_{\mathcal{X}_i}}(\xi_i\mathcal{N}(\mathcal{X}_i) - 1)\dot{\mathcal{X}}_i\end{aligned} \quad (57)$$

where $M_i = (\hat{\gamma}_{i,k} + \hat{\gamma}_{i,k+1})c\varepsilon_i + \frac{1}{4\mathcal{L}_i}D_i^2$, $C_i = 2min\{c_{i,1}, c_{i,2}, \cdots, c_{i,k+1}\}$, and $\frac{\partial g}{\partial u_i} = \xi_i$, $\left|\frac{\partial g}{\partial u}\right| = \left|\frac{4}{(e^{\frac{u}{u_M}}+e^{-\frac{u}{u_M}})^2}\right| \leq 1$.

By directly integrating differential inequality (57), we obtain:

$$V_{i,k+1} \leq V_{i,k+1}(0)e^{-C_i t} + \frac{1}{C_i}(M_i)(1-e^{-C_i t}) \\ \frac{e^{-C_i t}}{\gamma x_i}\int_0^t (\xi_i \mathcal{N}(\mathcal{X}_i) - 1)\,\dot{\mathcal{X}}_i e^{C_i \tau} d\tau \quad (58)$$

We can conclude that the closed-loop system is stable based on Lemma 1.

Theorem 1. Consider the uncertain nonlinear system (9) satisfying Assumptions 1– 3 and Lemma 1. An adaptive backstepping sliding mode control (49) makes outputs $y_i(t)$ track the desired trajectory $y_{d_i}(t)$ while ensuring the boundedness of all the closed-loop signals.

Proof: By applying the virtual controllers (25), (26), and (33), along with the Lyapunov functions (27), (41), and (52), and implementing the parameter update laws (39) and (40), and control law (49), the stability of the closed-loop system is ensured.

IV. Results and Discussion

In this section, we apply the proposed controller scheme to an uncertain bi-model SEIAR epidemiological model with five saturated control inputs. The system dynamics incorporate input saturation, uncertainty, and external disturbances. The values of the system parameters used in the simulations are sourced from references [4, 30], and are provided in Table 2. We validate the effectiveness of the proposed system through simulation analysis in the MATLAB Simulink environment. The performance of the proposed controller is compared with two other controllers: the dynamic anti-windup compensator (AWC) and the adaptive sliding mode controller (ASMC), as detailed in [20] and [15] respectively. In [20], the AWC addresses actuator saturation by employing a two-step design. First, a nonlinear feedback controller is developed without considering input constraints, and then a dynamic compensator is added to manage saturation This compensator leverages the difference between the generated control signal and the saturated signal as a dead-zone signal to activate the anti-windup mechanism. Additionally, we assume the following saturation levels for the control inputs:

$$sat(u_i) = \begin{cases} 0.75, & u_i \geq 0.75 \\ u_i, & 0 \leq u_i \leq 0.75,\ i = 1,2,3 \\ 0, & u_i \leq 0 \end{cases} \quad (59)$$

$$sat(u_i), = \begin{cases} 0.35, & u_i \geq 0.35 \\ u_i, & 0 \leq u_i \leq 0.35, i = 4,5 \\ 0, & u_i \leq 0 \end{cases} \quad (60)$$

TABLE II INTERPRETATION OF SYSTEM PARAMETERS [4, 30]

Parameter	Description	Values ($days^{-1}$)
ν	Rate of birth	0.0086
κ_1	Rate of becoming infectious after a latent period from E_1 to I_1	0.955
κ_2	Rate of becoming infectious after a latent period from E_2 to I_2	0.526
γ_1	The cure rate for the infected with comorbidity	0.633
γ_2	The cure rate for the infected with comorbidity	0.833
η_1	The cure rate for Asymptomatic class I	0.112
η_2	The cure rate for asymptomatic class II	0.244
p_1	Percentage of experiencing symptoms for class I	0.867
p_2	Percentage of experiencing symptoms for class II	0.667
β_1	Transmission rate from S to E_1	1.667
β_2	Transmission rate from S to E_2	1.667
μ	Natural death rate	0.0039
ω	Rate of losing immunity	0.833
ρ_1	Mortality rate of individuals caused by infection for class I	0.03
ρ_2	Mortality rate of individuals caused by infection for class II	0.02

The simulations are based on a final treatment time of $t_f = 60$ days, which represents the duration required to eradicate the disease from the population, as determined by the designer. The running time of algorithm implementation is 3.0101 seconds. To control the disease epidemic, the target reduction of the susceptible and infected compartments (I_d, E_d, S_d) over time is defined as follows:

$$S_d = (S_0 - S_f)\exp(-at) + S_f \\ E_{d_i} = (E_{0i} - E_{fi})\,exp(-at) + E_{f_i}, i = 1,2 \\ I_{d_i} = (I_{0i} - I_{fi})\,exp(-at) + I_{f_i} \quad (61)$$

Here, (a) is the adjustable population reduction rate, chosen as $a = 0.2$. The desired steady-state numbers of infected, exposed, and susceptible individuals denoted as I_{fi}, E_{fi}, and S_f are assumed to be zero ($i.e., I_f = 0$, $E_f = 0$, $S_f = 0$). The initial numbers of infected, exposed, and susceptible individuals are represented as I_0, E_0, and S_0 , respectively. respectively. The initial values of the influenza variables used in these simulations, along with the parameters for the controller, are provided in Tables 3 and 4, respectively. Additionally, the model parameters are perturbed by 80% , and $\Delta d(t) = [\,0.3\sin(4t)\ \ 0.5\sin(3t)\ \ 0.8\cos(2t)\ 0.2\sin(5t)\ 0.4\cos(t)]^T$

represents unidentified time-varying external disturbances, unmodeled dynamics, and perturbations introduced into the system.

TABLE III INITIAL VALUES OF THE STATE AND THE CONTROLLER VARIABLES

Variable	Initial value
$S(0)$	400
$E_1(0)$	120
$E_2(0)$	30
$I_1(0)$	150
$I_2(0)$	100
$A_1(0)$	50
$A_2(0)$	50
$R(0)$	100
$u(0)$	[1 0 1 1 0]
$\boldsymbol{\chi(0)}$	[0.01 0.0 0.02 0.02 0.01]

TABLE IV CONTROLLER PARAMETERS

Parameter	Description	Values
k	$[k_1\ k_2\ k_3\ k_4\ k_5]$	[20 10 10 30 20]
γ_x	$[\gamma_{x_1}\ \gamma_{x_2}\ \gamma_{x_3}\gamma_{x_4}\ \gamma_{x_5}]$	[0.01 0.01 0.01 0.1 0.11]
$\mathcal{L}$	$[\mathcal{L}_1\ \mathcal{L}_2\ \mathcal{L}_3\ \mathcal{L}_4\ \mathcal{L}_5]$	[5 10 20 10 10]
ε	$[\varepsilon_1\ \varepsilon_2\ \varepsilon_3\ \varepsilon_4\ \varepsilon_5]$	[1 1 1 10 10]

The text presents a comparative analysis of three simulation scenarios to investigate the population dynamics of the two-group SEIAR mathematical model under varying conditions. These scenarios encompass:

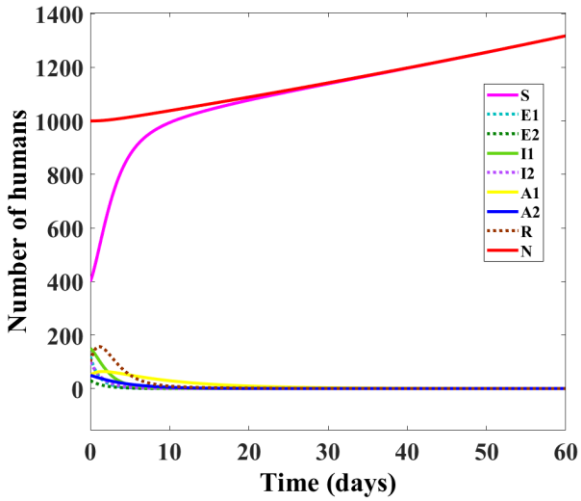
(I) Absence of control measures: This scenario serves as a baseline to observe the model's behavior without any interventions.

(II) Application of different controllers on an unconstrained System: Here, various controllers are applied to the model without considering any constraints. This allows for an assessment of the controllers' effectiveness in an ideal setting.

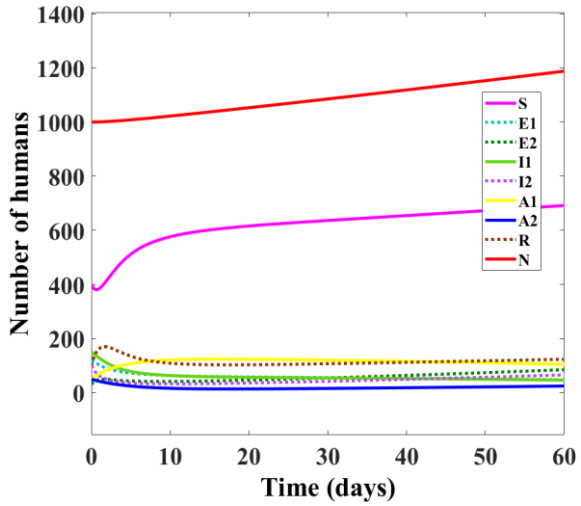
(III) Examination of the input-constrained System: in this scenario, the model incorporates input constraints, reflecting real-world limitations. The performance of the proposed dynamic compensator, AWC, and adaptive SMC is evaluated under these constraints.

The comparison of these scenarios provides insights into the impact of control strategies and saturation constraints on the population dynamics of the two-group SEIAR model. It highlights the need for careful controller design and consideration of practical limitations to achieve adequate disease. Fig.3 illustrates the temporal evolution of the populations under consideration in the absence of control measures. Numerical analysis is conducted for the susceptible, exposed, and infected classes, examining scenarios where $R_0 > 1$ and $R_0 < 1$.

Using the parameters from Table 2 and $\beta = 0.1$, the calculated basic reproduction numbers are $R_0^1 = 0.2248$ and $R_0^2 = 0.2364$. These values indicate that the infection dies out and the virus-free equilibrium is stable. In contrast, when $\beta = 1.667$, equations (7) and (8) yield $\mathrm{R}_0^1 = 3.7691$ and $\mathrm{R}_0^2 = 3.9643$, both greater than 1. Consequently, the disease becomes uniformly persistent, converging to an endemic equilibrium at (691, 47.2, 84.7, 46.3, 65.5, 104, 24.5, 123). As a result, the population will consistently contain infectious and asymptomatic individuals, implying that natural disease eradication is impossible. Therefore, control measures must be implemented to eradicate the disease. It is observed that R_0^1 is lower than R_0^2, indicating that individuals with comorbidities are more vulnerable to infection.



(a)



(b)

Fig.3. Open-loop response of the epidemic in the absence of control measures, when (a) $R_0 < 1$, and (b) $R_0 > 1$.

Figs. 4, 5, 6, and 7 illustrate the management of susceptible, recovered, exposed, and infected individuals in an unconstrained system under various control strategies. These figures highlight the dynamics of the epidemic compartments over time, providing a comprehensive view of how the disease evolves in response to different interventions. The implementation of these control strategies

leads to a significant and rapid decline in the basic reproduction number as the outbreak progresses. A lower R_0 signifies that each infected individual transmits the disease to fewer people, which is a critical factor in curbing an epidemic. Eventually, the model converges to a disease-free equilibrium, represented by $(0, 0, 0, 0, 0, 0, 0, N)$ as $t \to \infty$, indicating the effective eradication of the disease within the population.

As depicted in Fig. 4, the number of susceptible individuals decreases to zero, successfully achieving the intended tracking objective for this compartment. This decline suggests that the population has either recovered or acquired immunity, effectively disrupting the chain of transmission. Similarly, Fig. 5 illustrates that the number of recovered individuals steadily increases, asymptotically approaching the total population. This trend confirms a successful recovery process facilitated by the applied control mechanisms.

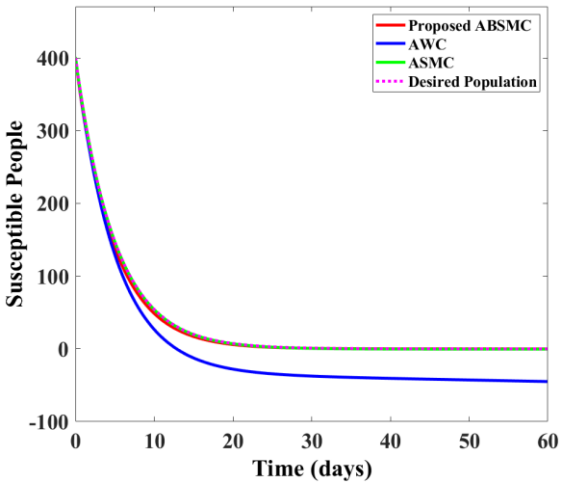


Fig.4. Changes in the number of susceptible individuals in the unconstrained system under different control strategies.

Figs. 6 and 7 present the variations in the number of exposed and infected individuals under different conditions, including scenarios with and without comorbidities. These figures emphasize how the control strategies effectively manage disease propagation in an unconstrained system. In both cases, the interventions significantly reduce the number of exposed and infected individuals over time, underscoring their efficacy in mitigating the epidemic.

This analysis highlights the importance of implementing appropriate control measures to combat infectious diseases and provides a robust framework for understanding the dynamics of disease transmission and recovery in various population groups.

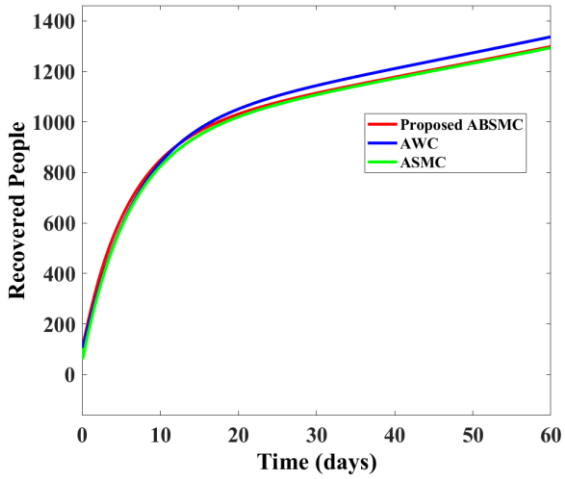
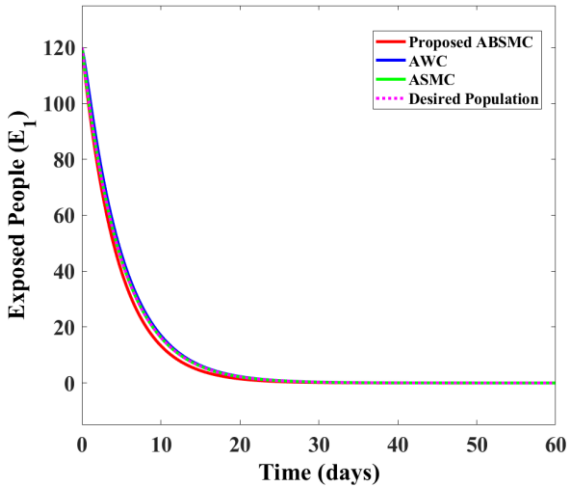
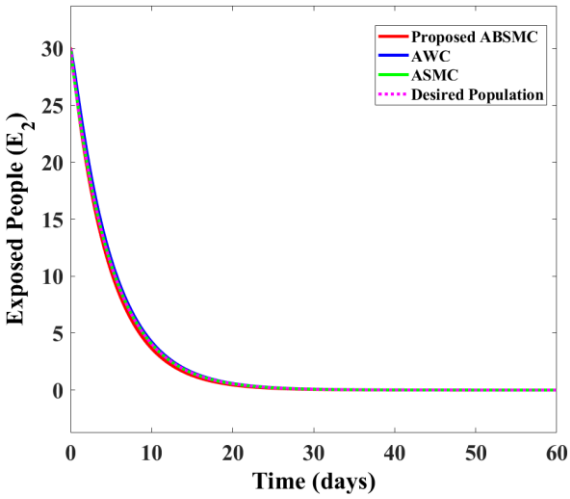


Fig.5. Changes in the number of recovered individuals in the unconstrained system under different control strategies.



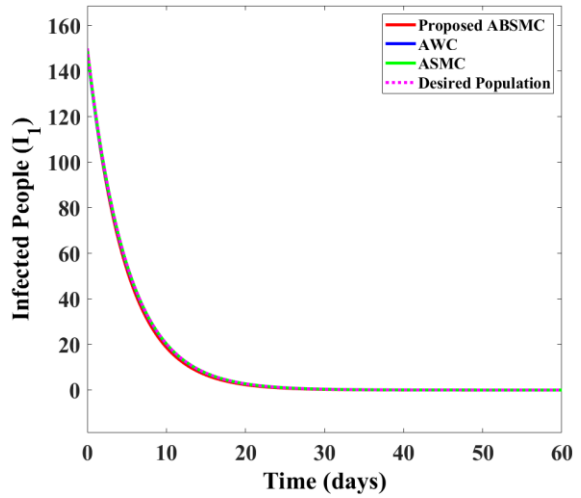
(a)



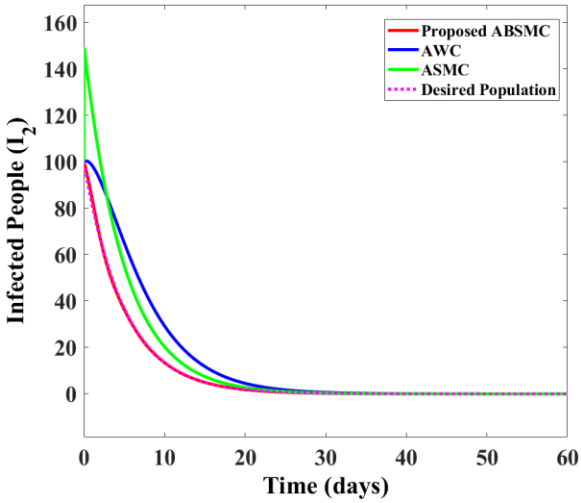
(b)

Fig.6. Changes in the number of exposed individuals in the unconstrained system under different control strategies: (a) with comorbidities and (b) without comorbidities.

However, as illustrated in Fig. 4, the anti-windup compensator (AWC) controller exhibits limitations in managing uncertainties and external disturbances, leading to the unrealistic prediction of a negative susceptible population. This drawback suggests that the AWC controller may not be fully effective in maintaining system stability under uncertain conditions. In contrast, the proposed controller demonstrates superior convergence speed, improved tracking accuracy, and greater robustness in handling the epidemic dynamics. These advantages highlight its effectiveness in optimizing disease control strategies and ensuring a more reliable response to outbreaks.



(a)



(b)

Fig.7.Changes in the number of infected individuals in the unconstrained system under different control strategies: (a) with comorbidities and (b) without comorbidities.

Now, consider a scenario where the control inputs are limited. When the actuator becomes saturated, feedback loops are disrupted, preventing the controller from effectively influencing system performance. Consequently, saturation issues can lead to significant performance degradation, resulting in oscillations, prolonged settling times, undershoots, delays, excessive overshoots, and instability. Figs. 8, 9, 10, and 11 illustrates the output of the constrained system under various control strategies after 60 days of treatment. As shown in Figs. 8 and 9, the degradation of the uncompensated system is evident in the output responses, which are characterized by undesirable oscillations and an extended settling time, ultimately compromising control performance. As a result, during the treatment period, a portion of the population remains susceptible, and recovered individuals are unable to fully converge to the total population.

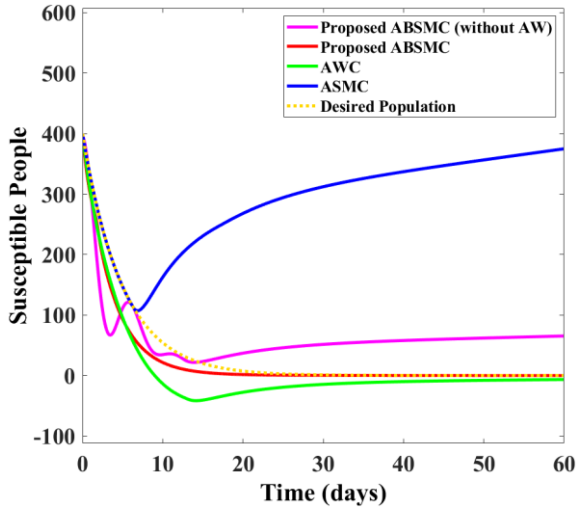


Fig.8. Change in the number of susceptible individuals in the input-constrained system under different control strategies.

After applying various control strategies to the constrained system, it is clear that overall system performance has improved. The ABSMC approach offers several advantages over other methods. It demonstrates superior tracking accuracy by minimizing tracking errors between actual system states and desired trajectories. ABSMC effectively handles input saturation, ensuring control inputs remain within feasible bounds while maintaining stability and performance. The approach provides enhanced stability by incorporating integral action to eliminate steady-state errors and improve overall stability, even in the presence of uncertainties and disturbances.

Additionally, as shown in Fig. 8, on the day 60, the difference in the number of susceptible individuals between the cases with and without the proposed ABSMC controller is approximately 66 individuals. This demonstrates that even when the vaccination input is saturated, the proposed controller effectively mitigates the negative impacts of input constraints and reduces the number of susceptible individuals.

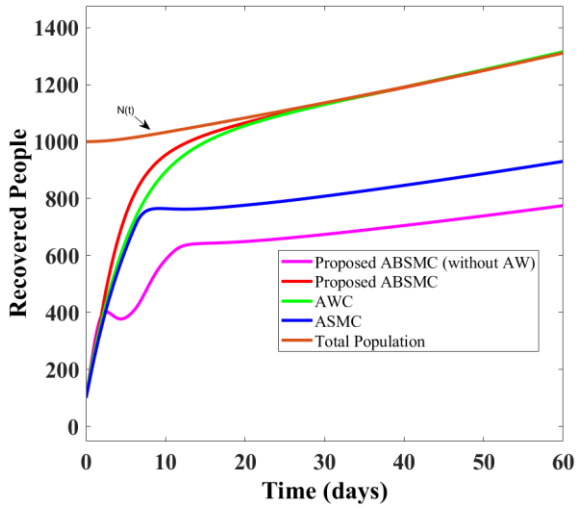
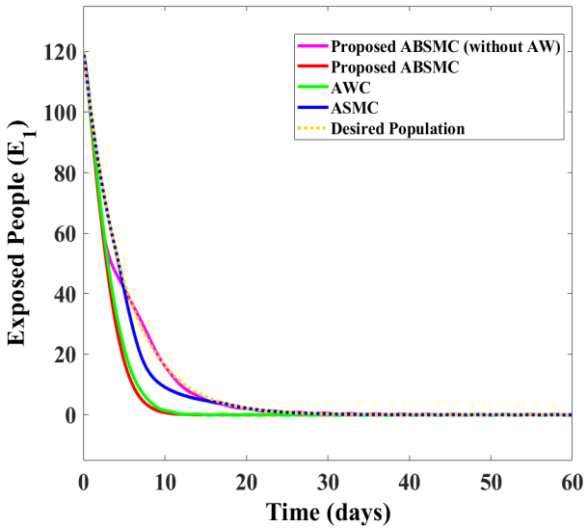


Fig.9. Change in the number of recovered individuals in the input-constrained system under different control strategies.

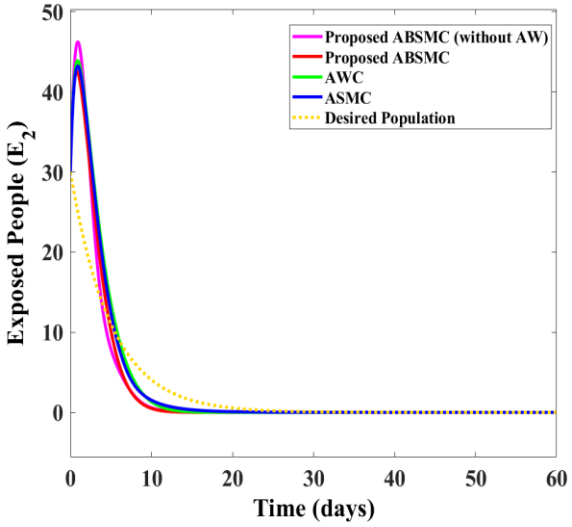
Furthermore, as illustrated in Fig. 9, when saturation occurs with the proposed controller, the number of recovered individuals increases over time and converges toward the final population. This behavior is due to the controller's ability to maintain stability and ensure that the system converges to the desired equilibrium point even in the presence of input saturation.

The proposed ABSMC compensator's effectiveness in handling input saturation is crucial in real-world scenarios, where resource limitations and practical constraints may restrict the implementation of control inputs. By mitigating the effects of saturation, the controller ensures that the epidemic model remains stable and converges to the desired disease-free equilibrium point, reducing the impact of the pandemic on the population.

Based on the information presented in Figs.10, and 11, the convergence rate to zero for infected and exposed individuals is faster when the proposed ABSMC compensator is employed compared to other methods. This is a crucial factor in managing pandemic diseases, as it is essential to control the timing of the disease to quickly steer the model toward a disease-free equilibrium point. The faster convergence rate achieved by the ABSMC compensator is attributed to its improved tracking accuracy, robustness to input saturation, enhanced stability, and adaptability. These advantages allow the ABSMC controller to respond effectively to changes in the epidemic dynamics and to drive the system towards the desired disease-free equilibrium point more rapidly. The implementation of the proposed compensator reduces the eradication duration of infected and exposed individuals by approximately 15 days compared to scenarios without it. By reducing the eradication duration of infected and exposed individuals, the ABSMC compensator can potentially mitigate the impact of the pandemic, reduce the burden on healthcare systems, and save lives.



(a)



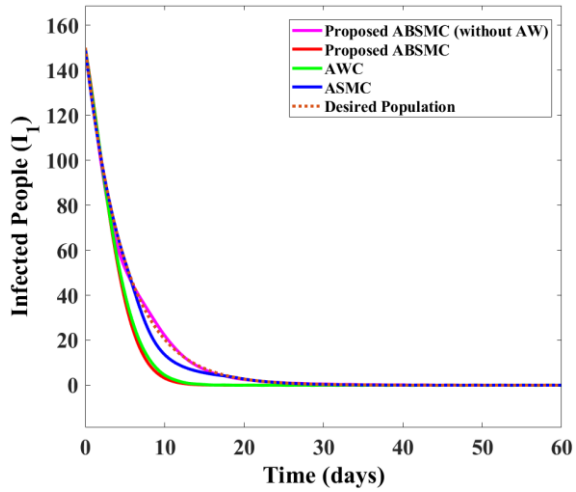
(b)

Fig.10. Change in the number of exposed individuals with and without comorbidities in the input-constrained system under different control strategies.

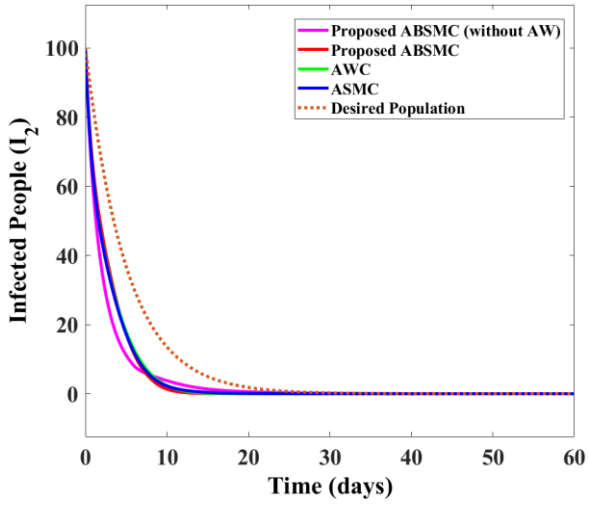
The implemented rates of vaccination for the susceptible compartments (u_1), social distancing for the exposed individuals (u_2, u_3), and antiviral treatment for the infected individuals (u_4, u_5) are illustrated in Figs. 12 and 13. It is important to note that the vaccination, social distancing, and antiviral treatment rates in this model must be less than $1 (0 \leq u_i(t) \leq 1, i = 1, \dots, 5)$. This constraint ensures that the control inputs remain within feasible ranges. The simulation results demonstrate that the obtained control inputs satisfy this implementation constraint. This ensures that the control strategies are practically implementable and do not violate any physical or biological constraints.

In the following, the impact of parametric uncertainty on the performance of the nonlinear robust adaptive controller is investigated. To this end, uncertainties of 20%, 40%, 60%

and 80% are applied to the initial estimation of model parameters ($\hat{\theta}$) relative to their real values (θ), as outlined in Table 2. Specifically, $\hat{\theta} = 1.2\theta, 1.4\theta, 1.6\theta$ and 1.8θ correspond to 20%, 40%, 60% and 80% uncertainty, respectively. The tracking errors for the susceptible, exposed, and infected populations—both with and without underlying diseases—under varying levels of uncertainty are depicted in Figs. 14, 15, 16, 17, and 18, respectively. As illustrated in these figures, the proposed controller effectively manages different degrees of parametric uncertainty. Even with an uncertainty level of 80%, the tracking errors remain bounded, ensuring system stability.



(a)



(b)

Fig.11. Change in the number of infected individuals with and without comorbidities in the input-constrained system under different control strategies

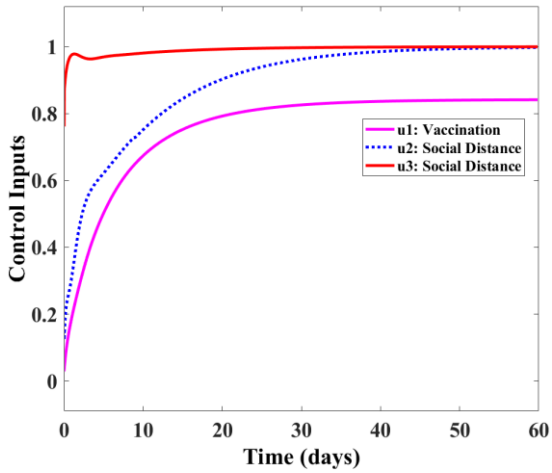


Fig. 12. The required rate of vaccination and social distancing applied to the two-group epidemic model

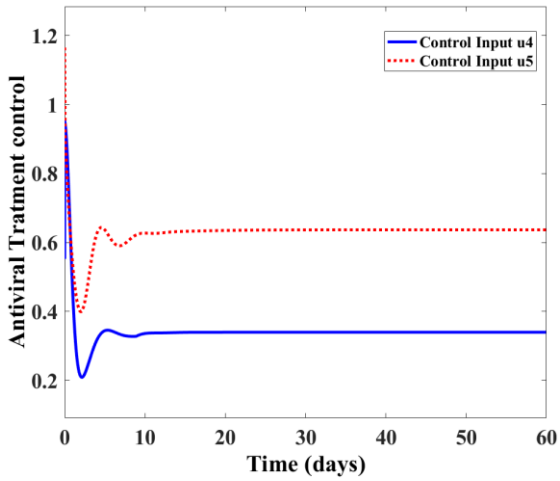


Fig. 13. The required rate of antiviral treatment applied to the two-group epidemic model

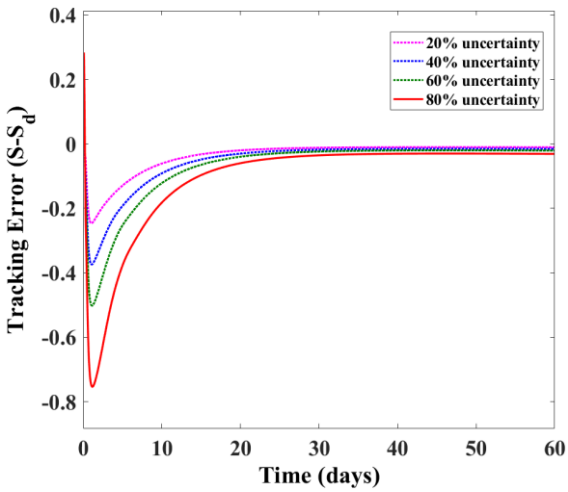


Fig. 14. The effect of 20%, 40%, 60% and 80% uncertainty in the estimated model parameters on tracking errors of the susceptible populations ($S - S_d$).

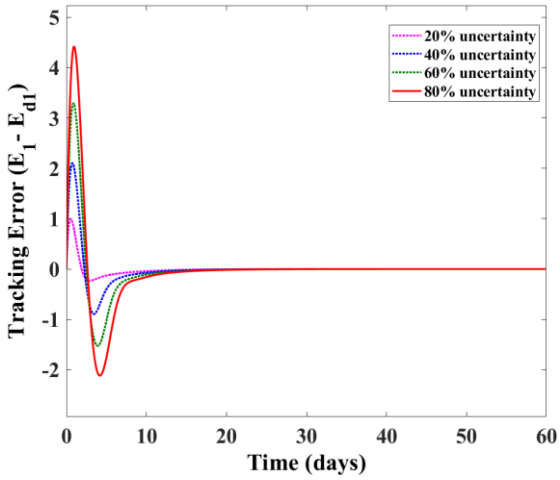


Fig.15. The effect of 20%, 40%, 60% and 80% uncertainty in the estimated model parameters on tracking errors of the exposed populations with comorbidities $(E_1 - E_{d_1})$.

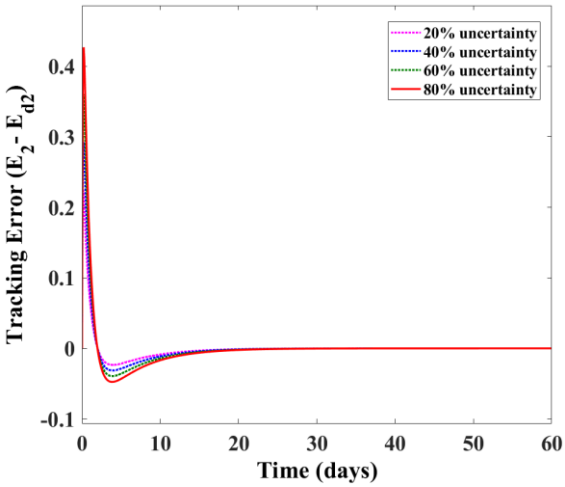


Fig.16. The effect of 20%, 40%, 60% and 80% uncertainty in the estimated model parameters on tracking errors of the exposed populations without comorbidities $(E_2 - E_{d_2})$.

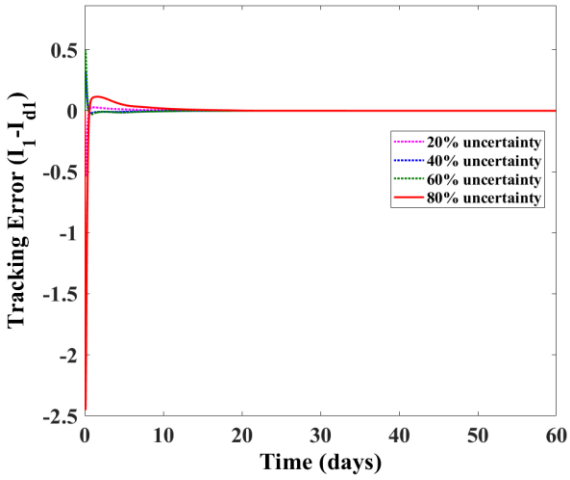


Fig. 17. The effect of 20%, 40%, 60% and 80% uncertainty in the estimated model parameters on tracking errors of the infected populations with comorbidities $(I_1 - I_{d_1})$.

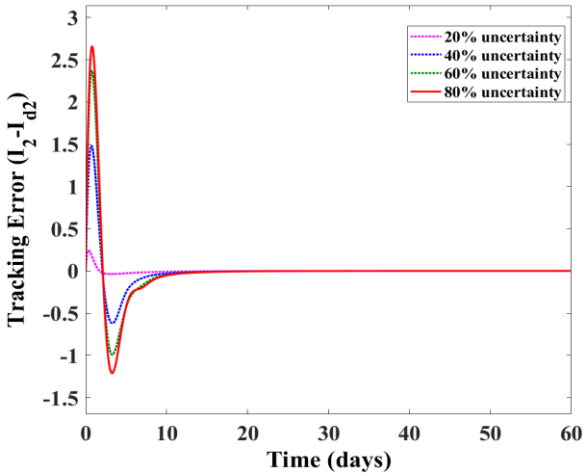


Fig. 18. The effect of 20%, 40%, 60% and 80% uncertainty in the estimated model parameters on tracking errors of the infected populations without comorbidities $(I_2 - I_{d_2})$.

These results underscore the robustness and adaptability of the proposed approach in handling uncertain system parameters while maintaining reliable performance.

To further evaluate the robustness of the proposed control approach, we investigate the required variation of vaccination, social distancing, and antiviral treatment in the control process of epidemic with different levels of uncertainty in model parameters. We consider three scenarios: 30%, 60%, and 90% uncertainty in model parameter compared to the nominal plant. As shown in Figs. 19, 20, and 21, the proposed control method effectively handles parameter uncertainty. Despite significant variations in the model parameters, the required control inputs remain within acceptable ranges, ensuring effective management of the epidemic. Therefore, the nonlinear control strategy demonstrates strong robustness against parametric uncertainties in the model.

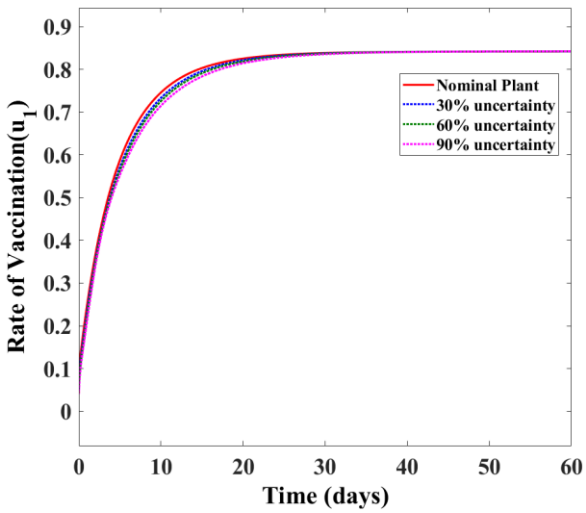
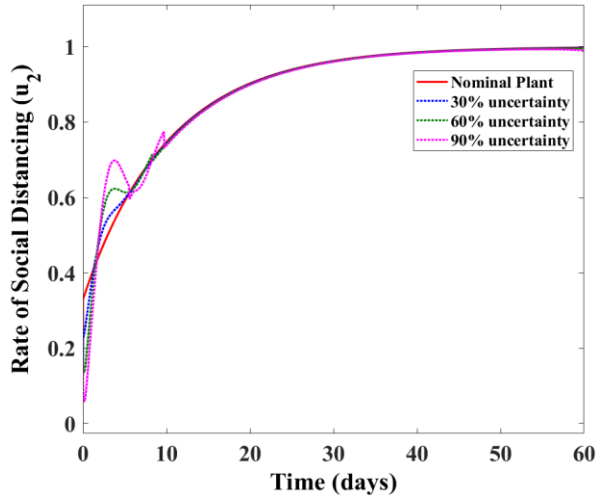
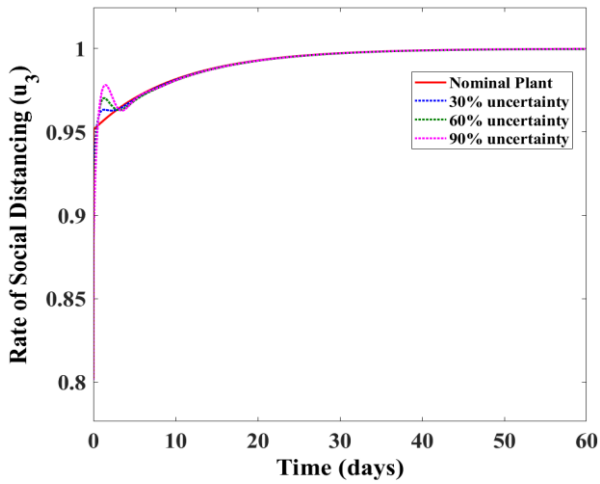


Fig. 19. Required variation of vaccination in control process of epidemic with 30%, 60% and 90% uncertainty in model parameters in comparison with the nominal plant.



(a)

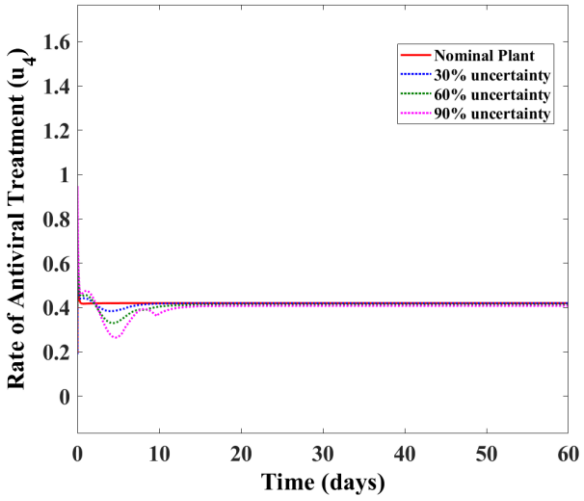


(b)

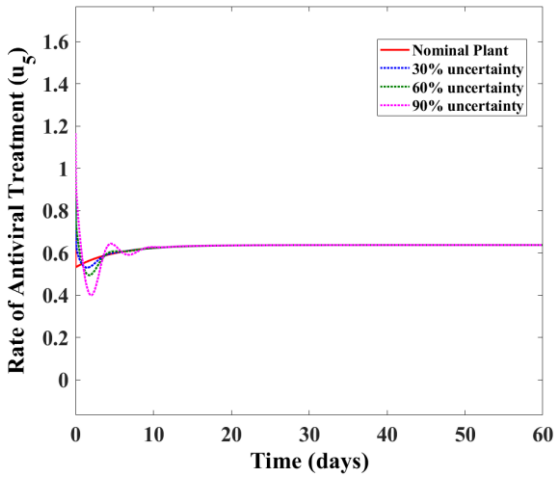
Fig. 20. Required variation of social distancing in control process of epidemic with 30%, 60% and 90% uncertainty in model parameters in comparison with the nominal plant.

In epidemic disease simulations, error bars serve a fundamental role in capturing the inherent uncertainty present in the model's predictions. They provide a visual representation of the variability in key epidemiological parameters, such as transmission rates, recovery rates, and other disease dynamics, under the influence of both model uncertainties and external disturbances. By including error bars that reflect both the mean and standard deviation, these simulations offer a more nuanced understanding of the reliability of the predictions, enabling the assessment of the potential range of outcomes rather than a single deterministic result.

This approach is particularly valuable when evaluating the effectiveness of intervention strategies, as it accounts for variations in real-world conditions, such as changes in public behavior, environmental factors, or external interventions. Moreover, error bars highlight the sensitivity of the model to fluctuations in parameter values, thus allowing researchers to identify critical parameters that most influence the disease progression. This information is essential for refining control strategies, ensuring that interventions remain robust even in the presence of substantial uncertainties.



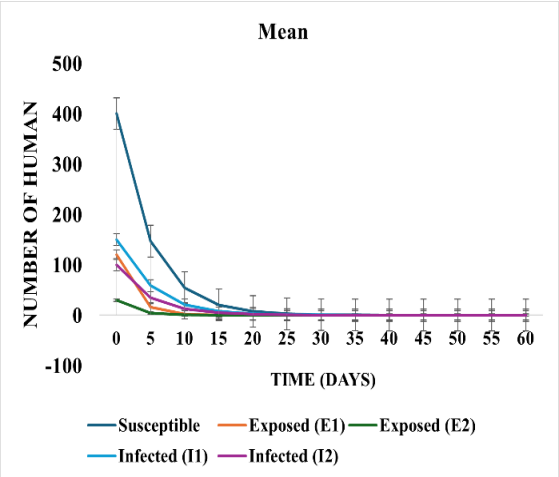
(a)



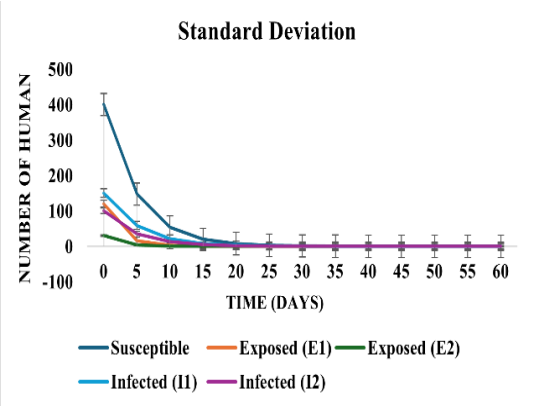
(b)

Fig. 21. Required variation of vaccination, social distancing, and antiviral treatment in control process of epidemic with 30%, 60% and 90% uncertainty in model parameters in comparison with the nominal plant.

Furthermore, the incorporation of error bars enhances the predictive power of the model by emphasizing the range of possible epidemic trajectories, thereby offering more realistic insights into the potential public health outcomes under varying levels of uncertainty. This aids policymakers in making informed decisions, particularly when there is a need to balance the trade-offs between control measures and their associated uncertainties. The error bars representing the mean and standard deviation of the simulation results are shown in Fig. 22, which visually underscores the uncertainty inherent in the model's predictions and highlights the variability in outcomes across different parameter scenarios.



(a)



(b)

Fig. 22. Error bars representing (a) the mean value and (b) the standard deviation for the population dynamics over time

V. Conclusions

This study investigates the effectiveness of an anti-windup compensation method in a MIMO epidemic system modeled as a positive system, with a particular focus on input saturation, modeling uncertainties, and external disturbances. It is the first study to explore these specific aspects within the context of epidemic modeling and control, this research addresses practical constraints by incorporating input saturation and employing an anti-windup compensation method, thereby enhancing the robustness and performance of the epidemic control system. The proposed nonlinear robust adaptive backstepping sliding mode control (ABSMC) strategy combines the advantages of adaptive sliding mode control and backstepping control to tackle the spread of epidemic diseases within a host population.

One of the key challenges addressed in this study is input saturation, which necessitates a careful balance between stability and precision. To achieve this balance, the research introduces a novel approach using auxiliary systems and Nussbaum gain functions. The Nussbaum function serves as a mathematical tool to address the nonlinearities caused by input saturation, ensuring the stability and positivity of system states while enhancing the controller's robustness. When integrated with the auxiliary design system, this approach creates a resilient and adaptive control scheme capable of performing effectively under various challenging conditions.

To model the spread of the disease, a two-group SEIAR epidemic model with uncertain parameters is utilized, incorporating dynamic population changes. By accounting for uncertainties in the model's nonlinear dynamics, the proposed controller is better equipped to manage variations and unexpected changes in the disease transmission process. This results in improved control performance and resilience in real-world scenarios. The control strategy focuses on reducing the numbers of susceptible, exposed, infected, and asymptomatic individuals to zero while maximizing the recovered population through effective tracking of the total population. Simulation results demonstrate that the proposed ABSMC control scheme effectively addresses the challenges posed by input saturation and external disturbances, ensuring the stability of the nonlinear uncertain MIMO epidemic system while achieving the desired trajectory tracking performance.

Furthermore, this control method can have significant social and economic impacts. By reducing the number of infected individuals and accelerating population recovery, treatment costs are reduced, and societal productivity is increased. Compared to traditional control methods, this new approach offers greater flexibility and resilience to uncertainties and disturbances, making it a suitable option for controlling epidemics in real-world conditions.

However, practical implementation faces certain challenges. In real-world situations, the number of individuals in each group may not be readily accessible, necessitating the development of control methods that rely on observer output for the epidemic model. Future studies will explore observer-based design methods and effective control strategies for nonlinear epidemic and biological systems. Additionally, to address the limitations identified in this study, future work will investigate alternative strategies for improving the controller's robustness and computational efficiency in resource-constrained environments. This includes examining the impact of larger-scale uncertainties and unmodeled dynamics on system performance. For example, integrating machine learning techniques could enhance parameter estimation and adaptability in real-time applications, further advancing the method's effectiveness.

References

[1] I. Sekkak, B. R. Nasri, B. N. Rémillard, J. Dzevela Kong and M. El Fatini , "A stochastic analysis of a SIQR epidemic model with short and long-term prophylaxis," Communications in Nonlinear Science and Numerical Simulation, vol. 127, p. 107523, 2023, doi: 10.1016/j.cnsns.2023.107523.

[2] T. Li, Y. Li , Y. Zhang, Y. Wang and X.-F. Luo, "A possible method of selecting spatial epidemic models based on Turing's diffusive threshold," Physica A: Statistical Mechanics and its Applications, vol. 624, p. 128986, 2023, doi: 10.1016/j.physa.2023.128986.

[3] Z. Abbasi, I. Zamani, A. H. Amiri Mehra, M. Shafieirad and A. Ibeas, "Optimal Control Design of Impulsive SQEIAR Epidemic Models with Application to COVID-19," Chaos, Solitons & Fractals, vol. 139, p. 110054, 2020, doi: 10.1016/j.chaos.2020.110054.

[4] A. H. Amiri Mehra, I. Zamani, Z. Abbasi and A. Ibeas, "Observer-based adaptive PI sliding mode control of developed uncertain SEIAR influenza epidemic model considering dynamic population," Journal of Theoretical Biology, vol. 482, p. 109984, 2019, doi: 10.1016/j.jtbi.2019.08.015.

[5] S. Muthukumar, A. Balakumar, S. Ravikumar and V. Chinnadurai, "An optimal control of bi-modal COVID-19 SEIQR epidemic spreading model in India," Results in Control and Optimization, vol. 12, p. 100256, 2023, doi: 10.1016/j.rico.2023.100256.

[6] J. Wang and . B. Dai, "Dynamical analysis of a multi-group SIR epidemic model with nonlocal diffusion and nonlinear incidence rate," Nonlinear Analysis: Real World Applications, vol. 68, p. 103661, 2022, doi: 10.1016/j.nonrwa.2022.103661.

[7] Y. Luo , L. Zhang, Z. Teng and T. Zheng, "Analysis of a general multi-group reaction–diffusion epidemic model with nonlinear incidence and temporary acquired immunity," Mathematics and Computers in Simulation, vol. 182, pp. 428-455, 2021, doi :10.1016/j.matcom.2020.11.002.

[8] A. I. Abioye, J. P. Olumuyiwa, A. O. Hammed, A. O. Festus, O. Kayode, A. I. Abdullahi and K. Ilyas, "Mathematical model of COVID-19 in Nigeria with optimal control," Results in Physics, vol. 28, p. 104598, 2021, doi: 10.1016/j.rinp.2021.104598.

[9] A. A. Khan, S. Ullah and R. Amin, "Optimal control analysis of COVID-19 vaccine epidemic model: a case study," The European Physical Journal Plus, vol. 137, pp. 1-25, 2022, doi: 10.1140/epjp/s13360-022-02365-8.

[10] N. R. Sasmita, M. Ikhwan, S. Suyanto and V. Chongsuvivatwong, "Optimal control on a mathematical model to pattern the progression of coronavirus disease 2019 (COVID-19) in Indonesia," Global Health Research and Policy, vol. 5, pp. 1-12, 2020, doi: 10.1186/s41256-020-00163-2.

[11] A. Srivastava and Nilam , "Optimal control of a fractional order SEIQR epidemic model with non-monotonic incidence and quarantine class," Computers in Biology and Medicine, vol. 178, p. 108682, 2024, doi: 10.1016/j.compbiomed.2024.108682.

[12] A. Veisi and H. Delavari, "Fractional-order backstepping strategy for fractional-order model of COVID-19 outbreak," Mathematical Methods in the Applied Sciences, vol. 45, no. 7, pp. 3479-3496, 2021, doi: 10.1002/mma.7994.

[13] A. Rajaei, M. Raeiszadeh, V. Azimi and M. Sharifi, "State estimation-based control of COVID-19 epidemic before and after vaccine development," Journal of Process Control, vol. 102, pp. 1-14, 2021, doi: 10.1016/j.jprocont.2021.03.008.

[14] A. Rajaei, A. Vahidi-Moghaddam, A. Chizfahm and M. Sharifi, "Control of malaria outbreak using a non-linear robust strategy with adaptive gains," IET Control Theory & Applications, vol. 13, no. 14, pp. 2308-2317, 2019, doi: 10.1049/iet-cta.2018.5292.

[15] M. Sharifi and H. Moradi, "Nonlinear robust adaptive sliding mode control of influenza epidemic in the presence of uncertainty," Journal of Process Control, vol. 56, pp. 48-57, 2017, doi: 10.1016/j.jprocont.2017.05.010.

[16] M. Wan, M. Chen and M. Lungu, "Integral Backstepping Sliding Mode Control for Unmanned Autonomous Helicopters Based on Neural Networks," Drones , vol. 7, p. 154, 2023, doi: 10.3390/drones7030154.

[17] M. A. M. Basri, "Design and application of an adaptive backstepping sliding mode controller for a six-DOF quadrotor aerial robot," Robotica, vol. 36, no. 11, pp. 1701-1727, 2018, doi: 10.1017/S0263574718000668.

[18] H. Shen, J. Iorio and N. Li, "Sliding Mode Control in Backstepping Framework for a Class of Nonlinear Systems," journal of Marine Science and Engineering, vol. 7, no. 12, p. 452, 2019, doi: 10.3390/jmse7120452.

[19] N. Adhikary and C. Mahanta, "Integral backstepping sliding mode control for underactuated systems: Swing-up and stabilization of the Cart–Pendulum System," ISA Transactions, vol. 52, pp. 870-880, 2013, doi: 10.1016/j.isatra.2013.07.012.

[20] S.S. Yoon, J.K. Park and T.W. Yoon, "Dynamic anti-windup scheme for feedback linearizable nonlinear control systems with saturating inputs," Automatica, vol. 44, no. 12, pp. 3176-3180, 2008, doi: 10.1016/j.automatica.2008.10.003.

[21] H. Eliasi, "Design an anti-windup controller for a PWR power-level control in the," Annals of Nuclear Energy, vol. 132, pp. 415-426, 2019, doi: 10.1016/j.anucene.2019.04.040.

[22] W. Guo and D. Liu, "Adaptive second-order backstepping control for a class of 2DoF underactuated systems with input saturation and uncertain disturbances," Scientific Reports, vol. 14, p. 15840, 2024, doi: 10.1038/s41598-024-66552-6.

[23] Y. Zhao, X. Sun, G. Wang and Y. Fan, "Adaptive Backstepping Sliding Mode Tracking Control for Underactuated Unmanned Surface Vehicle With Disturbances and Input Saturation," IEEE Access, vol. 9, pp. 1304-1312, 2020, doi: 10.1109/ACCESS.2020.3046130.

[24] S. Neisarian, M. M. Arefi, A. Abooee and S. Yin, "Fast finite-time observer-based sliding mode controller design for a class of uncertain nonlinear systems with input saturation," Information Sciences, vol. 630, pp. 599-622, 2023, doi: 10.1016/j.ins.2023.02.051.

[25] M. De la Sen, A. Ibeas and S. Alonso-Quesada, "On vaccination controls for the SEIR epidemic model," Commun Nonlinear Sci Numer Simulat, vol. 17, pp. 2637-2658, 2012, doi: 10.1016/j.cnsns.2011.10.012.

[26] A. K. Jain and S. Bhasin, "Robust backstepping control of uncertain nonlinear systems with unknown time-varying input delay," IFAC-PapersOnLine, vol. 53, no. 2, pp. 4862-4867, 2020, doi: 10.1016/j.ifacol.2020.12.1043.

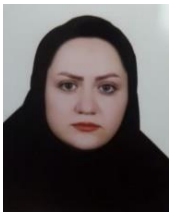
[27] Z. Chen, "Nussbaum functions in adaptive control with time-varying unknown," Automatica, vol. 102, pp. 72-79, 2019, doi: 10.1016/j.automatica.2018.12.035.

[28] Y. J. Liu and S. Tong, "Barrier Lyapunov functions for Nussbaum gain adaptive control of full state constrained nonlinear systems," Automatica, vol. 76, pp. 143-152, 2017, doi: 10.1016/j.automatica.2016.10.011.

[29] C. Wen, J. Zhou, .Z. Liu and H. Su, "Robust Adaptive Control of Uncertain Nonlinear Systems in the Presence

of Input Saturation and External Disturbance," IEEE Transactions on Automatic Control, vol. 56, pp. 1672-1678, 2011, doi: 10.1109/TAC.2011.2122730.

[30] A. Ibeas, M. de la Sen and S. Alonso-Quesada, "Robust Sliding Control of SEIR Epidemic Models," Mathematical Problems in Engineering, vol. 2014, p. 104764, 2014, doi: 10.1155/2014/104764.



Fariba Nobakht was born in Mashhad, Iran, in 1982. She received the B.Sc. degree in electronic engineering from Semnan University, Semnan, Iran, in 2006 and the M.Sc. degree in control engineering from Islamic Azad University, Gonabad branch, Gonabad, Iran, in 2010. Now, she is an Instructor of Asrar Institute of Higher Education, Mashhad, Iran. Her research interests include Positive Nonlinear System, Constrained Systems, Stability Analysis and Robust Control.



Hussein Eliasi received the B.S. degree in electrical engineering from the Ferdowsi University of Mashhad (FUM), Iran, in 2001. He received the M.S. and the Ph.D. degrees from Amirkabir University of technology (Tehran), Iran, in 2005 and 2011, respectively. He is currently an assistance professor in faculty of electrical engineering at University of Birjand, Iran. His research interests include Constrained Nonlinear Dynamics Systems, Robust Control, Parameter Optimization of Model Predictive Control, Transient Stability in Power Systems and Load Following by Nuclear Power Plants.